Applied Thermal Engineering 244 (2024) 122690

Contents lists available at ScienceDirect

Applied Thermal Engineering

journal homepage: www.elsevier.com/locate/apthermeng

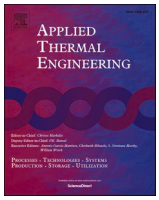

Research Paper

Energy influence of the internal heat exchangers placement in a cascade refrigeration plant. A theoretical and experimental analysis

Ramón Cabello *, Alejandro Andreu-Nácher, Daniel Sánchez, Rafael Larrondo

Jaume I University, Dep. of Mechanical Engineering and Construction, Campus de Riu Sec s/n, E-12071 Castellón, Spain

ARTICLE INFO

Keywords:
Internal heat exchanger
Cascade refrigeration system
R290
R1270
R1234ze(E)
R600a
R134a
CO2
Energy efficiency

ABSTRACT

This paper deals with the analysis of the internal heat exchanger (IHX) impact on the energy performance of a cascade refrigeration plant (CRS) made up of two vapor compression cycles. Three IHX locations have been considered, the first one in the high temperature cycle (HTC), the second one in the low temperature cycle (LTC), and the third one thermally connecting the suction line of the LTC with the liquid line of the HTC. Additionally, five refrigerant pairs R134a/R744, R290/R744, R1270/R134a, R600a/R744, and R1234ze(E)/R744 and three different heatsink temperatures: 293 K, 303 K and 313 K have been considered. The experimental results, obtained in a CRS experimental facility, are contrasted with those obtained from a theoretical model. While theoretical results predict that the IHXs have mainly negative or neglecting effects on the energy performance of the CRS, the experimental ones results show that regardless of location and operating conditions, the activation of an IHX generally improves the COP, up to 5.6 % as a maximum improvement.

1. Introduction

Despite its paramount importance, the refrigeration sector is in the spotlight because it accounts for 7.8 % of global greenhouse gas emissions. These emissions can be split into 63 % due to the high consumption of electrical energy (called indirect effect) and a 37 % due to the leakage of fluorinated gases into the atmosphere (called direct effect) [8,20]. Fluorinated gases regulations such as the Kigali amendment to the Montreal Protocol [11], or the [17] approved by European Commission [F-Gas 2015] aim to reduce the direct effect. But, once the use of low GWP refrigerants is spreading out, the impact of indirect emissions prevails in the accounting of total CO_{2eq} emissions. Therefore, as of 2017, approximately 80 % of the climate impact of cooling equipment came from indirect emissions. So, to achieve further greenhouse effect mitigation, the indirect effect, must also be addressed, and this should be done by increasing the energy performance of the refrigeration facilities as is pointed out by many assessments, like [10] or [7].

Cooling plants with Booster or Cascade architectures are commonly used to meet the growing demand for low evaporating temperature in commercial, industry and health refrigeration applications. Focusing on cascade refrigeration system (CRS), the most recent regulations on fluorinated gases have conditioned the refrigerants used in them. However, the selection of a suitable refrigerant pair, affects not only to the direct effect but also to the indirect effect, because the working fluids pairing has a great influence on the energy performance of the CRS. In this sense, several research have been published in which it has been evaluated the most adequate low-GWP refrigerants. Among the most recent theoretical works we can cite one by [9], who studied the selection of hydrocarbon refrigerants, concluding that the best performance is achieved with the pair Trans-2-butane in the LTC and Toluene in the HTC, being able to replace other pairs including R23, R404A, R13 or R41, and another by [19], who investigated the use of low GWP refrigerant pairs like NH3/CO2, R1234yf/CO2, and R1234ze/CO2, obtaining that NH3/CO2 performs better than the other pairs. In the experimental field, it is worth to mention the recent works by [5] and [2]. Both have carried out a wide range of tests in CRS to evaluate different alternatives to R134a as refrigerant in the HTC, using R744 as refrigerant in the LTC. The first one tackles with hydrocarbons family fluids (R290, R1270 and R600a) and with R1234ze(E), concluding from a TEWI analysis, that all these alternative refrigerants achieve reductions in CO_{2eq} emissions, also finding that R290 improves the performance of the CRS by an average of 2.15 % for low and medium heat sink temperatures (20–30 °C). The second work, that from [2], tackles with R513A, R1234yf and R436A, concluding that all the alternative fluids achieve reductions in TEWI with respect to R134a, and that only R436A (R290/R600a, 54/46 %w) achieves average increase in the CRS

* Corresponding author.
E-mail address: cabello@uji.es (R. Cabello).

https://doi.org/10.1016/j.applthermaleng.2024.122690
Received 27 April 2023; Received in revised form 8 January 2024; Accepted 7 February 2024
Available online 12 February 2024

Nomenclature

COP	coefficient of performance
CRS	Vapor Compression Cascade Refrigeration System
HTC	High-Temperature Cycle
HX_{cc}	Cascade Heat Exchanger
IHX	Internal Heat Exchanger
LTC	Low-Temperature Cycle
$\dot{m}$	Mass Flow rate ($kg \cdot s^{-1}$)
$\dot{V}$	Volumetric Flow rate ($m^3 \cdot s^{-1}$)
p	Pressure, (kPa)
P_C	Compressor power consumption, (kW)
$\dot{Q}_O$	cooling capacity (kW)
q_o	Specific cooling capacity ($kJ \cdot kg^{-1}$)
qv	Volumetric cooling capacity ($kJ \cdot m^{-3}$)
c_p	Specific heat capacity ($kJ \cdot kg^{-1} \cdot K^{-1}$)
T	Temperature (K)
r_c	Compressor pressure ratio
SHSL	Super Heat in compressor Suction Line
T_{HS}	Heat sink temperature (°C)
v	Specific volume ($m^3 \cdot kg^{-1}$)
w_c	Specific compression work ($kJ \cdot kg^{-1}$)

GREEK SYMBOLS

Δ	Prefix, means preceding variable variation
η_v	Compressor volumetric efficiency
η_G	Compressor global efficiency
ρ	Density ($kJ \cdot m^{-3}$)

SUBSCRIPTS

cc	Cascade
dis	Compressor discharge
exp	Expansion
glyc	Glycol
H	Hight temperature
i	Inlet
Is	Isentropic
K	Condensing level
L	Low temperature
O	Evaporating level
o	Outlet
ref	Refrigerant
suct	Compressor suction
w	Water

coefficient of performance of 3.1 %.

But the selection of the working fluids should not be the only way to improve the energy performance of the CRS. One of the most cost-effective methods to improve the energy performance of single-stage vapor compression cycles is the connection of an IHX. Its effects have been studied in different vapor compression architectures. For instance, [3,4], states that improvements occur in all tested scenarios when the IHX is connected in a horizontal freezing cabinet. The cabinet ran with a single stage vapor compression cycle, and was tested with refrigerants R404A, R290, R1270, R454C, R455A, R468A, R290, R1270, R454C, R455A and R468A. The reduction in energy consumption reached 9.2 %. Furthermore, improvements were found to increase as the heat sink temperature increases. In the research presented by [14], three different locations of the IHX in a transcritical CO2 Booster system are theoretically analysed. They conclude that greatest performance improvements (6.36 %) are achieved when the IHX is located at the suction line of the

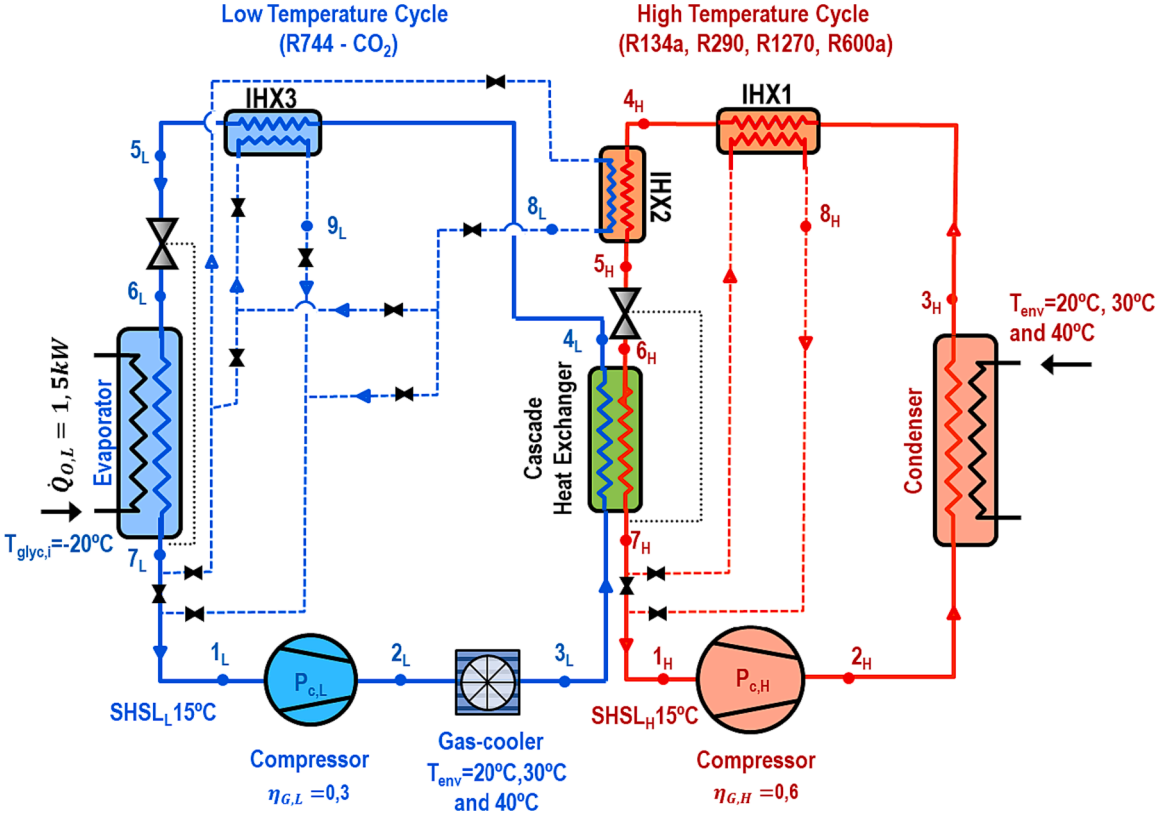

Fig. 1. Scheme of the modelled cascade refrigeration plant.

Table 1
Phase change temperatures in theoretical model.

$T_{env.}$	20 °C	30 °C	40 °C
$T_{k,H} = T_{env.} + 7$ÂºC	27 °C	37 °C	47 °C
$T_{3L} = T_{env} + 2$ÂºC	22 °C	32 °C	42 °C
$T_{k,L}$	−9°C	−5°C	−1°C
$T_{O,H} = T_{k,L} - 5$ÂºC	−14 °C	−10 °C	−6°C
$T_{O,L} = T_{glyc,i} - 10$ÂºC	−30 °C	−30 °C	−30 °C

high-pressure stage compressor, also allowing the reduction of the optimal gas-cooler pressure. Llopis et al. [15] examined the effects caused by the use of an IHX in the LTC of a cascade refrigeration system working with R134a/R744. The experimental results confirmed that IHX can slightly reduce the cooling capacity and improve the overall COP value by up to 3.7 %.

Apart from the last work cited above, as far as the cascade refrigeration systems are concerned, no other works dealing with IHX in CRS have been found in the literature. Although they are used since Tellier proposed this system in 1867, there is still a lack of information,

Table 2
Main results of the energy parameters obtained from the theoretical model.

Refrigerant pair	Heat sink temp.	IHX			q_{vH} (kJ·m^{-3})	q_{vL} (kJ·m^{-3})	$\dot{Q}_{OH}$(kW)	P_{cH} (kW)	P_{cL} (kW)	COP_H (-)	COP_L (-)	COP (-)
R134a/R744	20	BASE	58.2	78.7	1257	8737	1.679	0.396	0.428	4.243	3.508	1.822
		IHX1	65.6	78.7	1266	8737	1.679	0.398	0.428	4.216	3.508	1.816
		IHX2	58.2	126.2	1500	7511	1.679	0.332	0.533	5.063	2.817	1.736
		IHX3	58.2	92.6	1257	8622	1.625	0.383	0.445	4.243	3.373	1.812
	30	BASE	68.9	97.6	1355	8440	1.729	0.492	0.542	3.512	2.766	1.450
		IHX1	77.6	97.6	1370	8440	1.729	0.494	0.542	3.497	2.766	1.447
		IHX2	68.9	157.3	1691	7068	1.729	0.394	0.693	4.385	2.166	1.380
		IHX3	68.9	116.5	1355	8312	1.655	0.471	0.567	3.512	2.648	1.445
	40	BASE	79.2	116.2	1437	8136	1.782	0.605	0.666	2.948	2.254	1.181
		IHX1	89.2	116.2	1464	8136	1.782	0.605	0.666	2.946	2.254	1.181
		IHX2	79.2	188.6	1889	6644	1.782	0.460	0.871	3.875	1.722	1.127
		IHX3	79.2	140.3	1437	8002	1.688	0.572	0.697	2.948	2.151	1.181
R290/R744	20	BASE	57.0	78.7	1847	8737	1.679	0.395	0.428	4.246	3.508	1.822
		IHX1	64.1	78.7	1860	8737	1.679	0.397	0.428	4.227	3.508	1.818
		IHX2	57.0	126.2	2036	7511	1.679	0.359	0.533	4.681	2.817	1.683
		IHX3	57.0	92.6	1847	8622	1.625	0.383	0.445	4.246	3.373	1.813
	30	BASE	67.5	97.6	1937	8440	1.729	0.494	0.542	3.498	2.766	1.447
		IHX1	75.9	97.6	1962	8440	1.729	0.495	0.542	3.491	2.766	1.446
		IHX2	67.5	157.3	2193	7068	1.729	0.437	0.693	3.959	2.166	1.328
		IHX3	67.5	116.5	1937	8312	1.655	0.473	0.567	3.498	2.648	1.443
	40	BASE	77.7	116.2	2001	8136	1.782	0.611	0.666	2.919	2.254	1.175
		IHX1	87.3	116.2	2042	8136	1.782	0.609	0.666	2.926	2.254	1.177
		IHX2	77.7	188.6	2336	6644	1.782	0.523	0.871	3.407	1.722	1.076
		IHX3	77.7	140.3	2001	8002	1.688	0.578	0.697	2.919	2.151	1.176
R1270/R744	20	BASE	63.4	78.7	2253	8737	1.679	0.408	0.428	4.119	3.508	1.796
		IHX1	70.8	78.7	2262	8737	1.679	0.411	0.428	4.084	3.508	1.788
		IHX2	63.4	126.2	2479	7511	1.679	0.371	0.533	4.532	2.817	1.661
		IHX3	63.4	92.6	2253	8622	1.625	0.394	0.445	4.119	3.373	1.788
	30	BASE	74.7	97.6	2361	8440	1.729	0.508	0.542	3.402	2.766	1.428
		IHX1	83.4	97.6	2380	8440	1.729	0.512	0.542	3.378	2.766	1.423
		IHX2	74.7	157.3	2665	7068	1.729	0.450	0.693	3.840	2.166	1.313
		IHX3	74.7	116.5	2361	8312	1.655	0.487	0.567	3.402	2.648	1.424
	40	BASE	85.6	116.2	2436	8136	1.782	0.627	0.666	2.843	2.254	1.161
		IHX1	95.6	116.2	2472	8136	1.782	0.629	0.666	2.832	2.254	1.158
		IHX2	85.6	188.6	2834	6644	1.782	0.539	0.871	3.307	1.722	1.064
		IHX3	85.6	140.3	2436	8002	1.688	0.594	0.697	2.843	2.151	1.162
R600a/R744	20	BASE	49.1	78.7	680	8737	1.679	0.379	0.428	4.432	3.508	1.860
		IHX1	56.1	78.7	687	8737	1.679	0.378	0.428	4.447	3.508	1.863
		IHX2	49.1	126.2	754	7511	1.679	0.342	0.533	4.914	2.817	1.716
		IHX3	49.1	92.6	680	8622	1.625	0.367	0.445	4.432	3.373	1.849
	30	BASE	58.5	97.6	735	8440	1.729	0.471	0.542	3.669	2.766	1.480
		IHX1	66.7	97.6	746	8440	1.729	0.468	0.542	3.697	2.766	1.485
		IHX2	58.5	157.3	836	7068	1.729	0.414	0.693	4.178	2.166	1.356
		IHX3	58.5	116.5	735	8312	1.655	0.451	0.567	3.669	2.648	1.474
	40	BASE	67.5	116.2	783	8136	1.782	0.577	0.666	3.089	2.254	1.207
		IHX1	77.0	116.2	801	8136	1.782	0.570	0.666	3.130	2.254	1.214
		IHX2	67.5	188.6	919	6644	1.782	0.492	0.871	3.626	1.722	1.101
		IHX3	67.5	140.3	783	8002	1.688	0.546	0.697	3.089	2.151	1.206
R1234ze(E)/R744	20	BASE	49.8	78.7	926	8737	1.679	0.381	0.428	4.413	3.508	1.856
		IHX1	57.1	78.7	937	8737	1.679	0.381	0.428	4.412	3.508	1.856
		IHX2	49.8	126.2	1123	7511	1.679	0.314	0.533	5.353	2.817	1.773
		IHX3	49.8	92.6	926	8622	1.625	0.368	0.445	4.413	3.373	1.845
	30	BASE	59.8	97.6	996	8440	1.729	0.477	0.542	3.626	2.766	1.472
		IHX1	68.4	97.6	1015	8440	1.729	0.475	0.542	3.639	2.766	1.474
		IHX2	59.8	157.3	1270	7068	1.729	0.374	0.693	4.623	2.166	1.406
		IHX3	59.8	116.5	996	8312	1.655	0.456	0.567	3.626	2.648	1.466
	40	BASE	69.5	116.2	1057	8136	1.782	0.589	0.666	3.026	2.254	1.196
		IHX1	79.4	116.2	1086	8136	1.782	0.584	0.666	3.053	2.254	1.200
		IHX2	69.5	188.6	1425	6644	1.782	0.437	0.871	4.081	1.722	1.147
		IHX3	69.5	140.3	1057	8002	1.688	0.558	0.697	3.026	2.151	1.195

especially experimental data [1]. Therefore, this paper is aimed to address this shortcoming by carrying out a comprehensive experimental study of the influence of IHX on the energy performance of the cascade refrigeration systems. In order to do so, three different locations for the IHX have been tested, namely IHX1, which thermally connects the HTC liquid and suction lines, IHX3, which thermally connects the LTC liquid and suction lines, and IHX2, which thermally connects the suction line of the low temperature cycle with the liquid line of the high temperature cycle. Regardless of the location of the IHX, it has an influence on the energy parameters of both cycles, this influence is explained and measured over a wide temperature range for the heat sink (20–40 °C) and a single temperature of −20 °C for the heat source. To extend the scope of this work, the tests are repeated under the same conditions, charging the CRS with five different refrigerant pairs R134a/R744, R290/R744, R1270/R744, R600a/R744 and R1234ze(E)/R744. We have selected this set of refrigerants because they represent the different families currently used, the HFCs, the HFOs and the HCs. The last have been identified as climate-friendly alternatives to fluorinated gases in many refrigeration applications (Climate Action - https://climate.ec.europa.eu/eu-action/fluorinated-greenhouse-gases/climate-friendly-alternatives-hfcs_en).

2. Basic thermodynamic model results

Previous to the tests, we have modelled the cascade refrigeration system (CRS) based on the first and second thermodynamic principles to compare the theoretical results with the experimental ones when the IHXs are activated. The scheme of the modelled plant is shown in Fig. 1.

The model has been developed using Eqs. (1)–(18), and the following inputs: 1.5 kW as cooling load, −20 °C as heat source temperature, 20 °C, 30 °C and 40 °C as heat sink temperatures, 15 °C as superheating in the suction lines of both cycles, 5 °C as superheating at the outlet of both evaporators, 2 °C as subcooling at the outlet of both condensers, 0.6 as global compressor efficiency in the HTC, 0.3 as compressor global efficiency in the LTC. Once the model and its input parameters were stablished, we evaluated the performance of the CRS for each of the three IHX activated individually.

Thermal effectiveness values of $\varepsilon_{IHX1} = 0.2$, $\varepsilon_{IHX2} = 0.6$ and $\varepsilon_{IHX3} = 0.6$ have been considered in this simulation part. To complete the theoretical analysis, we ran the model considering the same set of input parameters with the five pairs of refrigerants used in the experimental part: R134a/R744, R290/R744, R1270/R744, R600a/R744 and R1234ze(E)/R744.

The four phase change temperatures involved in the CRS have been stablished as a function to the heat source and heat sink temperatures. These values are used to stablish the working pressures in both cycles. In addition, temperature difference of 2 K between the environmental temperature and the refrigerant gas cooler outlet temperature has been considered. Their final values are shown in Table 1.

The temperatures at the outlet of the evaporators and condensers (7L, 4L, 7H, 3H) are calculated applying the superheating and subcooling values, the temperatures of states 8H, 8L and 9L are obtained from the thermal effectiveness of the IHXs, using Eqs. (1), (2) and (3). To calculate the suction temperatures (1L and 1H), the values of the superheating at the suction lines are used.

$$\varepsilon_{IHX1} = \frac{h(T_{8H};p_{OH}) - h(T_{7H};p_{OH})}{h(T_{3H};p_{kH}) - h(T_{7H};p_{OH})} \tag{1}$$

$$\varepsilon_{IHX2} = \frac{h(T_{8L};p_{OL}) - h(T_{7L};p_{OL})}{h(T_{4H};p_{kH}) - h(T_{7L};p_{OL})} \tag{2}$$

$$\varepsilon_{IHX3} = \frac{h(T_{9L};p_{OL}) - h(T_{7L};p_{OL})}{h(T_{4L};p_{kL}) - h(T_{7L};p_{OL})} \tag{3}$$

The compressor discharge temperatures are obtained from the isentropic discharge temperatures and the compressor global efficiencies. The values of the compressor global efficiencies considered are the average of those obtained experimentally (0.3 for LTC compressor, and 0.6 for HTC compressor). Finally, the thermodynamic properties of the states that define the CRS were calculated using Refprop v10 [13]. Once the thermodynamic properties were calculated, the energy parameters were evaluated using the set of Eqs. (4)–(18).

$$q_{o,L} = h_{7L} - h_{6L} \tag{4}$$

$$\dot{m}_{ref,L} = \dot{Q}_{o,L} \cdot q_{o,L}^{-1} \tag{6}$$

$$q_{o,H} = h_{7H} - h_{6H} \tag{5}$$

$$\dot{Q}_{o,H} = \dot{Q}_{k,L} \tag{7}$$

$$\dot{Q}_{k,L} = \dot{m}_{ref,L} \cdot (h_{3L} - h_{4L}) \tag{8}$$

$$\dot{m}_{ref,H} = \dot{Q}_{o,H} \cdot q_{o,H}^{-1} \tag{9}$$

$$h_{2L} = h_{1L} + \frac{h_{2sL} - h_{1L}}{\eta_{GL}} \tag{10}$$

$$h_{2H} = h_{1H} + \frac{h_{2sH} - h_{1H}}{\eta_{GH}} \tag{11}$$

$$w_{c,L} = h_{2L} - h_{1L} \tag{12}$$

$$w_{c,H} = h_{2H} - h_{1H} \tag{13}$$

$$P_{c,L} = \dot{m}_{ref,L} \cdot w_{c,L} \tag{14}$$

$$P_{c,L} = \dot{m}_{ref,L} \cdot w_{c,L} \tag{14}$$

$$P_{c,H} = \dot{m}_{ref,H} \cdot w_{c,H} \tag{15}$$

$$COP_L = \frac{q_{o,L}}{w_{c,L}} \tag{16}$$

$$COP_H = \frac{q_{o,H}}{w_{c,H}} \tag{17}$$

$$COP = \frac{\dot{Q}_{o,L}}{P_{c,H} + P_{c,L}} \tag{18}$$

The main results obtained with the theoretical model, related to compressor discharge temperatures and energy parameters, are given in Table 2. According with the model algorithm the IHX1and the IHX3 only affect the cycle where they are mounted, that is, the HTC and the LTC respectively, having no influence on the other cycle.

Thus, compared with the BASE configuration, the IHX1 produces increments around 12 % to 15 % in T_{disH} and around 1 % to 3 % in the q_{vH}, what means a large superheat in the suction line that practically counteracts the subcooling effect. For its part, the $\dot{Q}_{o,H}$ does not vary when IHX1 is connected, because in the model's algorithm the increasing in q_{oH} is balanced by the decreasing in the $\dot{m}_{ref,H}$ in the HTC, while the P_{cH} suffers very low variations, minor than ± 1 %. In this last case the decrease in $\dot{m}_{ref,H}$ compensates the increase of the specific compression work, $w_{c,H}$. In consequence, the COP_H has the same trend as P_{cH}, showing low reductions with R134a, R290 and R1270, and low increments with R600a and R1234ze(E). The COP values have the same trend as COPH but with lower values, so the theoretical energy impact of the IHX1 in the CRS is mighty low, with maximum increase of 0.61 % in case of R600a and minimum decrease of −0.34 % in case of R1270.

Regarding energy behaviour of the CRS operating with IHX3 compared with BASE configuration, the former generates an important rise in the LTC compressor discharge temperature, ranging from 17.7 %

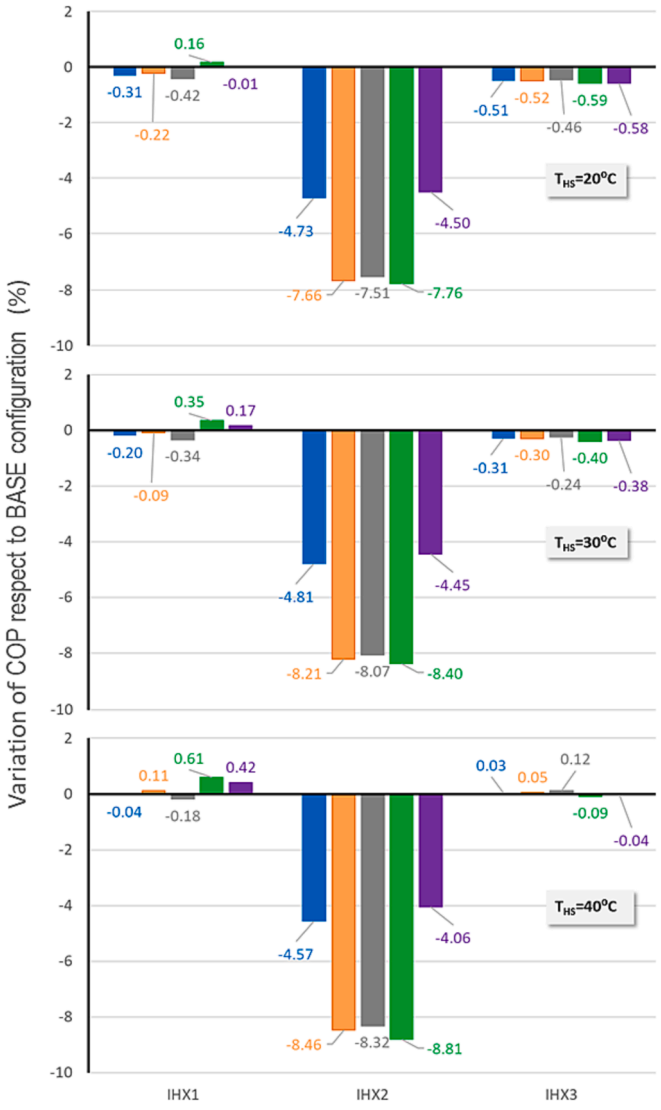

Fig. 2. Relative COP variation respect CRS configuration with none IHX activated, at THS = 20 °C and THS = 40 °C. $\varepsilon_{IHX2} = 0.6$.

to 20.75 % at 20 °C and 40 °C of $T_{env.}$ respectively. The q_{vL} is reduced by a maximum of 1.65 % at 40 °C of $T_{env.}$, which indicates that the specific volume increase in the suction line due to the superheating produced by the IHX3 is higher than the subcooling produced in the liquid line, which is the responsible for the increase in the specific cooling capacity. The P_{cL} increases between 4 % and 5 % driven by the specific work increase, despite the reduction in $\dot{m}_{ref,L}$. Therefore, as $\dot{Q}_{o,L}$ is a constant inlet parameter, the COP_L is reduced by a value varying from −3.85 % to −4.55 % at 20 °C and 40 °C of $T_{env.}$ respectively. Finally, the COP of the CRS also goes down but in lower extent than COP_L, the maximum reduction being −0.59 % using R1234ze(E) at 20 °C of $T_{env.}$

The last IHX to analyse its effect on the CRS is the IHX2. This heat exchanger affects both cycles, producing a subcooling in the HTC liquid line and a superheating in the LTC suction line. Compared to the BASE configuration, the IHX2 produces a significant increment in the T_{disL}, around 61 % and none in the T_{disH}. Regarding the volumetric cooling capacities, on the one hand the subcooling in the liquid line of the HTC generates a great increment in q_{vH} that oscillates from around 10 % to around 17 % when the evaluated refrigerants are hydrocarbons, and from around 20 % to around 35 % when the evaluated refrigerants are HFCs, on the other hand, the superheating in the suction line of the LTC generates reductions in the q_{vL} that range between −14 % and −18 %. The P_{cH} decreases due to the reduction of $\dot{m}_{ref,H}$, between −9% and −14 % in case of hydrocarbons and from −16 % to −25 % in case of HFCs, but the P_{cL} increases in a greater extent (-25 % to −30 %) due to the higher increase in w_L. These facts drive to an increase in the COP_H and a decrease in the COP_L, the final result being that the global COP of the CRS suffers a reduction by about −8% for hydrocarbons, and by about −4% for HFCs. The variations are always greater the higher the T_{env}.

To summarize the results, in the Fig. 2 the relative COP variations when each IHX is activated are depicted respect to the values calculated for CRS configuration without IHX activated. The results shown in Fig. 2 indicate that the activation of the IHX2 causes the COP to decrease significantly with all the refrigerant pairs, and over the entire range of heat sink temperatures. Activation of IHX3 produces small reductions in COP, lower than 0.6 %, with all refrigeration pairs, while activation of IHX1 leads to small increases with refrigerants R600a and R1234ze(E), and small decreases with R134a, R290 and R1270. The COP variations obtained when IHX1 or IHX3 are active are negligible in both cases.

In this theoretical model several assumptions and simplifications have been made, such as the influence of the IHX in the heat transfer rate in the heat exchangers or the effects on the compression vapor cycles where the IHX is not placed. Therefore, in the following sections, an experimental study has been conducted. The results obtained from this study take into account all the variables and effects involved when each IHX is connected.

3. Experimental set-up description and test methodology

3.1. Experimental set-up description and configurations used

Fig. 3 show a general picture of the CRS inside the climatic chamber. The scheme of the cascade refrigeration system used in this project and the location of the sensors are outlined in Fig. 4. It consists of two single stage vapor compression cycles thermally connected by a cascade heat exchanger (HX_{cc}). The high temperature cycle (HTC) is charged with 3.5 kg of working fluid (R134a, R290, R1270, R600a and R1234ze(E)) and is equipped with a semi-hermetic reciprocating compressor (BITZER 2HES-1Y-40S in case R134a, DORIN H-80CC in case of R290 and R1270, BITZER 2EC-2-2Y-40S at 1450 rpm in case R600a and 1116.5 rpm in case R1234ze(E)), an oil separator tank (Temprite 3358 in case R290 and R1270, ESK OS-12 in case R134a, R600a and R1234ze(E)), a welded plate heat exchanger as condenser (model: B15THx30; manufacturer: SWEP) with 0.952 m^2 of heat exchange surface, a refrigerant accumulation tank of 5 litter capacity, an electronic expansion valve (model: E2V09; manufacturer: CAREL) with thermostatic regulation which keeps 7 K of refrigerant superheating at evaporator outlet and a welded plate heat exchanger as evaporator (model: B8THx20; manufacturer: SWEP) with 0.414 m^2 of heat transfer surface. The heat exchanger acting as evaporator in the HTC is the thermal connection of both refrigeration circuits, acting as the LTC condenser as well, that is why we call it the HXcc.

Likewise, the low temperature cycle (LTC) is charged with 5.5 kg of R744 and is equipped with a is a semi-hermetic type reciprocating compressor (model CD150H; manufacturer: DORIN) with a displacement of 1.12 $m^3 \cdot h^{-1}$ at 1,450 rpm, an oil separator tank (Model: 133A, manufacturer: Temprite), a cross flow heat exchanger acting as gas cooler (model: LCE-213; manufacturer: ECO) equipped with an axial fan powered with a 76 W electric motor, the gas-cooler has 0.6 m^2 and 3.36 m^2 of internal and external heat transfer surfaces respectively, the previously mentioned HXcc being the condenser in the LTC, a 16 litter refrigerant accumulation tank, electronic expansion valve (model: E2V05; manufacturer: CAREL) with thermostatic regulation which keeps 7 K of refrigerant superheating at evaporator outlet and a welded plate heat exchanger operating as evaporator (model: B15THx20; manufacturer: SWEP) with 0.612 m^2 of heat transfer surface.

Additionally, three internal heat exchangers are mounted at the

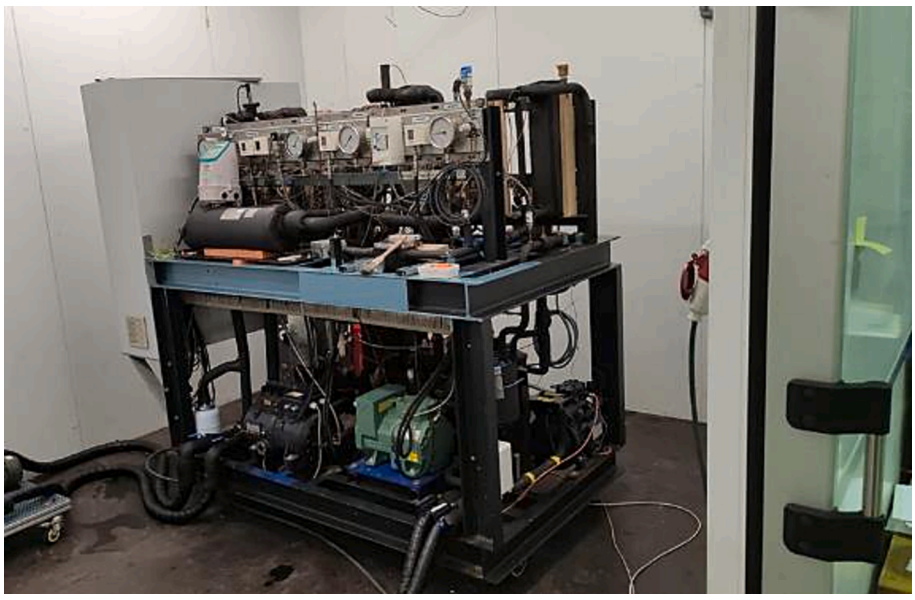

Fig. 3. General view of the experimental cascade refrigeration plant.

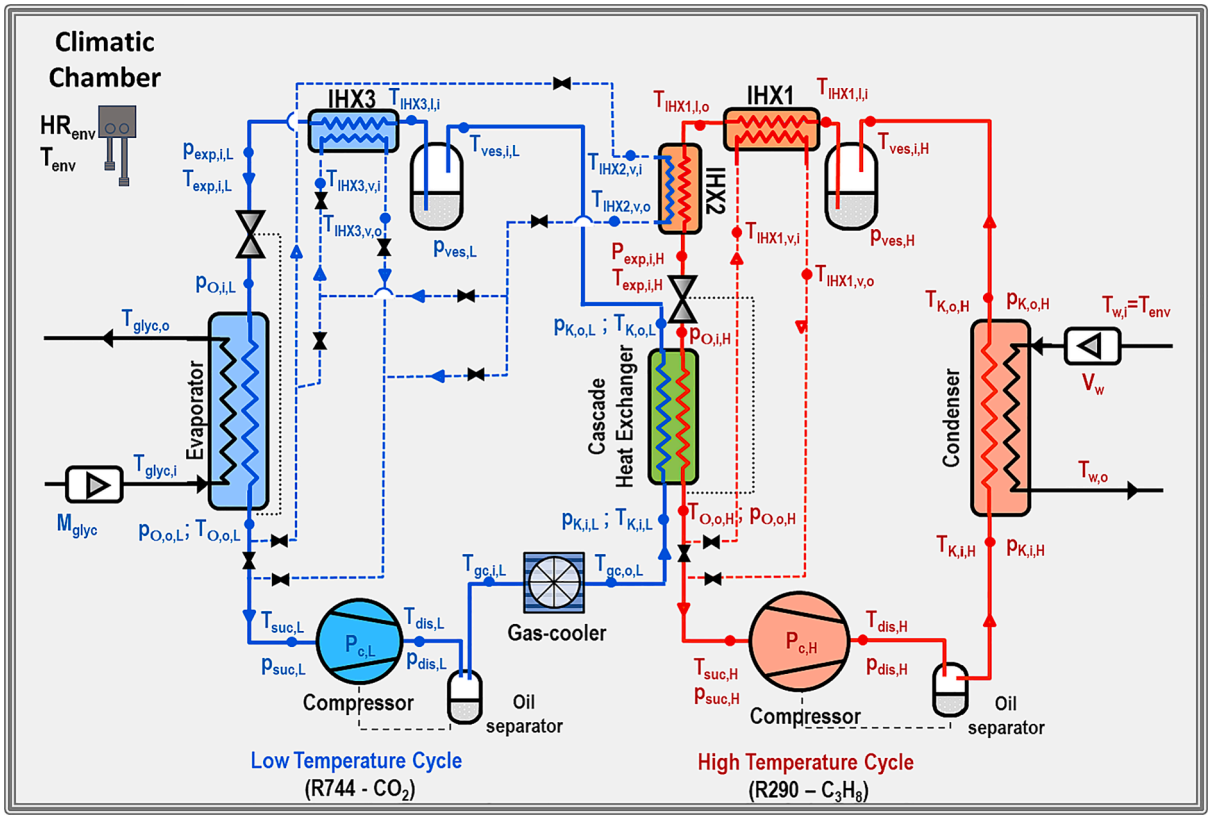

Fig. 4. CRS scheme.

locations shown in Fig. 4. These IHXs are double pipe type, with counter-current flow arrangement, and correspond to the HXR50 model from manufacturer Packless (0.0084 m^2 of internal heat transfer surface).

Refrigerants mass charges are an issue that is out of the scope of this work, which is aimed to analyse the energy behaviour. The refrigerant receivers placed in low and high temperature cycles make the energy performance of the system independent of the refrigerant charge.

Two auxiliary thermal rigs and a climatic chamber complete the experimental facility. One of the auxiliary thermal rigs and the climatic chamber, where the CRS is located, act as heat rejection sink providing a constant volumetric flow rate of water at three different temperatures (20 °C, 30 °C and 40 °C) to the HTC condenser and keeping the same indoor air temperature. The other thermal rig act as heat source by supplying a constant mass flow rate of a water and ethylene glycol mixture (50 %/50 % vol.) to the LTC evaporator at a constant temperature of −20 °C.

The CRS has been devised with the possibility of working with up to eight different configurations. In this paper we deal with four of them:

Table 3
Characteristics and accuracy of the measurement elements.

Number	Variable	Type	Calibration range	Accuracy
34	Temperature	T-type thermocouple	−40 to 125 °C	± 0.5 °C
4	Pressure	Pressure gauge. JOHNSON CONTROLS P499	0 to 30 bar	± 0.08 bar
3	Pressure	Pressure gauge. JOHNSON CONTROLS P499	0 to 16 bar	± 0.045 bar
4	Pressure	PMA GmbH. Transmitter P30/P31	0 to 50 bar	± 0.15 bar
3	Pressure	PMA GmbH. Transmitter P30/P31	0 to 60 bar	± 0.18 bar
1	Pressure	PMA GmbH. Transmitter P30/P31	0 to 100 bar	± 0.3 bar
1	Mass flow rate	Coriolis flow meter. YOKOGAWA ROTAMASS RCCT34	0 to 0.1 $kg{\cdot}s^{-1}$	± 0.1 % lecture
1	Volumetric flow rate	Magnetic flow meter. YOKOGAWA RXF032G	0 to 2.5 $m^3{\cdot}h^{-1}$	± 0.25 % lecture
2	Electric Power	Digital Wattmeter SENECA K109S	0 to 3,000 W	± 0.5 % lecture

Table 5
Equations used to calculate the main energy parameters.

$T_{O,L} = \frac{T_{sat.}\left(p_{O,i,L}\right) + T_{sat.}\left(p_{O,o,L}\right)}{2}$	Eq. (18)	$T_{O,H} = \frac{T_{sat.}\left(p_{O,i,H}\right) + T_{sat.}\left(p_{O,o,H}\right)}{2}$	Eq. (19)
$T_{K,L} = \frac{T_{sat.}\left(p_{K,i,L}\right) + T_{sat.}\left(p_{K,o,L}\right)}{2}$	Eq. (20)	$T_{K,H} = \frac{T_{sat.}\left(p_{K,i,H}\right) + T_{sat.}\left(p_{K,o,H}\right)}{2}$	Eq. (21)
$\Delta T_{cc} = T_{K,L} - T_{O,H}$	Eq. (22)	$r_c = \frac{p_{dis.}}{p_{suct.}}$	Eq. (23)
$q_O = h_{O,o} - h_{O,i}$	Eq. (24)	$w_C = h_{dis.} - h_{suct.}$	Eq. (25)
$\dot{Q}_{glyc} = \dot{m}\hat{A}\cdot(c_{p,in}\hat{A}\cdot T_{in} - c_{p,out}\hat{A}\cdot T_{out})\big\vert_{glyc}$	Eq. (26)	$\dot{Q}_w = \dot{V}\hat{A}\cdot\overline{\rho}\hat{A}\cdot\overline{c_p}\hat{A}\cdot(T_{out} - T_{in})\big\vert_w$	Eq. (27)
$\dot{m}_{ref,L} = \frac{(h_{O,o,L} - h_{O,i,L})}{\dot{Q}_{glyc}}$	Eq. (28)	$\dot{m}_{ref,H} = \frac{(h_{K,o,H} - h_{K,i,H})}{\dot{Q}_w}$	Eq. (29)
$\dot{Q}_{K,L} = \dot{m}_{ref,L}\hat{A}\cdot(h_{K,o,L} - h_{K,i,L})$	Eq. (30)	$\dot{Q}_{O,H} = \dot{m}_{ref,H}\hat{A}\cdot(h_{O,o,H} - h_{O,i,H})$	Eq. (31)
$\eta_{G,L} = \frac{\dot{m}_{ref,L}\cdot(h_{is,dis,L} - h_{suct,L})}{P_{c,L}}$	Eq. (32)	$\eta_{G,H} = \frac{\dot{m}_{ref,H}\cdot(h_{is,dis,i,H} - h_{suct,H})}{P_{c,H}}$	Eq. (33)
$\varepsilon_{IHX1} = \frac{T_{IHX1,v,i} - T_{IHX1,v,o}}{T_{IHX1,l,i} - T_{IHX1,v,i}}$	Eq. (34)	$\varepsilon_{IHX2} = \frac{T_{IHX2,v,i} - T_{IHX2,v,o}}{T_{IHX1,l,o} - T_{IHX2,v,i}}$	Eq. (35)
$\varepsilon_{IHX3} = \frac{T_{IHX3,v,i} - T_{IHX3,v,o}}{T_{IHX3,l,i} - T_{IHX3,v,i}}$			Eq. (36)
$\Delta T_{IHX,liq} = T_{IHX,l,o} - T_{IHX,l,i}$	Eq. (37)	$\Delta T_{IHX,vap} = T_{IHX,v,o} - T_{IHX,v,i}$	Eq. (38)
$COP_H = \frac{\dot{Q}_{O,H}}{P_{c,H}}$	Eq. (39)	$COP_L = \frac{\dot{Q}_{O,L}}{P_{c,L} + P_{gc}}$	Eq. (40)
$COP = \frac{\dot{Q}_{O,L}}{P_{c,L} + P_{c,H} + P_{gc}}$			Eq. (41)

BASE, IHX1, IHX2 and IHX3.

The BASE configuration is the one in which no IHX operates. The other three configurations are those in which only the IHX with the corresponding number is connected, according to the nomenclature shown in Fig. 4. The IHX1 is located on the HTC, immediately downstream the refrigerant receiver, and thermally connects the liquid and the suction lines of the HTC. The IHX3 is located in the LTC between the refrigerant receiver and the expansion valve. It thermally connects liquid and suction lines of the LTC. The IHX2 is placed immediately upstream of the HTC expansion valve. It thermally connects the LTC suction line with the HTC liquid line. So, the IHX2 brings into thermal contact both circuits, likewise the HXcc does.

Finally, there are four additional configurations resulting from the activation of more than one internal exchanger. These are combinations of the IHXs described above: IHX1 + IHX3, IHX1 + IHX2, IHX2 + IHX3 and IHX1 + IHX2 + IHX3. For reasons of length and comprehensiveness, they are going to be analysed in a separate article.

3.2. Measurement system and uncertainties

The refrigeration plant is fully equipped with pressure and temperature sensors, as well as with fluid flow meters and watt meters, to determine the thermodynamic states of the working fluids and the energy behaviour of the cascade facility. In Fig. 4, the location of these measurement equipment is shown. In Table 3 are gathered the characteristics of the sensors.

The uncertainties of the measurements are treated as described in [5]. For the direct parameters, i.e., pressure, temperature, flow rates and electrical consumptions, the standard deviations (u_σ), and the accuracy of the measurement devices (u_M) have been considered. The formers have been calculated from the measured data collection, and the latter have been taken from manufacturer's data. These both uncertainties have been used to estimate the total uncertainty (u_D) of direct parameters by using the expression proposed in [6]. For the thermodynamic properties (u_{TH}), the uncertainty has been estimated using the methodology proposed by [16].

3.3. Experimental procedure

The tests lasted 20 min of steady-state running, with the test plant being monitored every 5 s, which results in 240 data per sensor.

Throughout the test campaign, a water ethylene glycol mixture (50 %/50 % in volume) was used as the cooling load or heat source, with a mass flow rate of 0.111 $kg{\cdot}s^{-1}$ and a temperature of −20 °C (the

Table 4
Average values and corresponding uncertainties of heat sink and heat source parameters during all tests.

Configurations	T_{HS} (°C)	$T_{climatic\ chamber}$ (°C)	$T_{w,i}$ (°C)	$T_{w,o}$ (°C)	$T_{glyc,i}$ (°C)	$T_{glyc,o}$ (°C)	$\dot{m}_{glyc}$ $(kg{\cdot}s^{-1})$	$\dot{V}_w$ $(dm^3{\cdot}s^{-1})$
BASE	20	20.0 ± 0.52	20.0 ± 0.52	27.2 ± 0.53	−19.9 ± 0.60	−24.7 ± 0.58	402.0 ± 3.20	0.266 ± 0.0016
	30	30.1 ± 0.53	29.9 ± 0.53	37.3 ± 0.52	−19.9 ± 0.57	−24.5 ± 0.56	401.2 ± 3.16	0.266 ± 0.0014
	40	39.8 ± 0.54	39.9 ± 0.53	47.5 ± 0.52	−20.0 ± 0.53	−24.3 ± 0.53	403.1 ± 1.38	0.266 ± 0.0014
IHX1	20	19.9 ± 0.52	20.2 ± 0.51	27.0 ± 0.52	−19.9 ± 0.59	−24.8 ± 0.56	399.7 ± 3.16	0.266 ± 0.0016
	30	29.8 ± 0.52	30.0 ± 0.52	37.1 ± 0.52	−19.9 ± 0.56	−24.6 ± 0.55	399.4 ± 2.78	0.267 ± 0.0014
	40	39.6 ± 0.54	39.9 ± 0.52	47.3 ± 0.52	−19.9 ± 0.53	−24.3 ± 0.53	401.3 ± 1.89	0.266 ± 0.0013
IHX2	20	20.0 ± 0.54	20.1 ± 0.52	26.8 ± 0.52	−20.0 ± 0.60	−24.8 ± 0.57	400.1 ± 3.43	0.266 ± 0.0016
	30	30.2 ± 0.55	29.9 ± 0.52	36.7 ± 0.53	−20.0 ± 0.56	−24.5 ± 0.56	401.5 ± 2.66	0.266 ± 0.0013
	40	40.0 ± 0.57	40.1 ± 0.52	47.0 ± 0.52	−20.0 ± 0.53	−24.5 ± 0.53	401.7 ± 1.20	0.264 ± 0.0013
IHX3	20	20.0 ± 0.51	19.9 ± 0.52	27.0 ± 0.53	−20.0 ± 0.60	−24.9 ± 0.58	400.2 ± 3.25	0.266 ± 0.0016
	30	30.2 ± 0.52	29.9 ± 0.52	37.2 ± 0.53	−20.0 ± 0.56	−24.6 ± 0.56	400.0 ± 2.58	0.265 ± 0.0014
	40	40.0 ± 0.55	39.9 ± 0.52	47.4 ± 0.52	−19.9 ± 0.53	−24.3 ± 0.54	399.9 ± 1.42	0.265 ± 0.0013

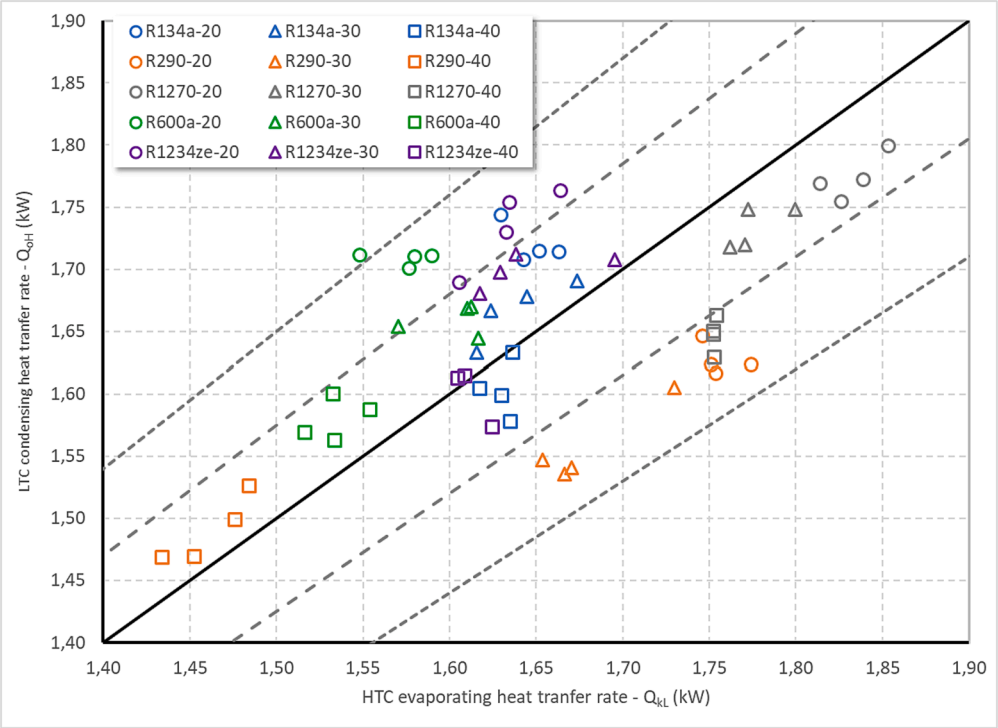

Fig. 5. Accuracy in the energy balance at the cascade heat exchanger.

common one for freezing applications). While as heat sink, both a water stream with a volumetric flow of 0.263 $m^3 \cdot h^{-1}$ was used for the HTC condenser, and the inside air of the climatic chamber for the LTC gas cooler. In the latter case, a 75 W fan forced the air movement through the gas cooler coil. The above cited parameters were kept constant in every test performed, while heat sink temperatures of 20 °C, 30 °C and 40 °C were tested for each CRS configuration. The described procedure is repeated with the five refrigerant pairs.

The actual inlet and outlet average temperatures of the secondary fluids used as heat sink and heat source, as well as, their respective volumetric and mass flow rates obtained throughout tests done with the five refrigerant pairs are summarized at Table 4, together with their average standard deviations. Their stability demonstrates the validity of the tests performed. In this table, $T_{climatic\ chamber}$ and T_{wi}, are the actual heat sink temperatures in the LTC gas-cooler and the HTC condenser, respectively.

4. Data reduction

The set of equations listed in Table 5, together with the measured data, are used to calculate all cycle parameters involved in the energy characterization of the CRS. The thermodynamic properties of all the working fluids involved in this work were calculated using Refprop v.10 [13], while SecCool v1.33 [12] software was used to calculate the density and the specific heat of secondary fluids (water in the case of the condenser and water-ethylene glycol blend in the case of evaporator).

The nomenclature of the pressure and temperature variables used in equations 18 to 41, corresponds to those shown in Fig. 4. The enthalpies are calculated at their respective pressures and temperatures, except the enthalpy at evaporator inlet, which is equal to the enthalpy at the expansion valve inlet. Data validation

Fig. 5 shows the accuracy of the measurements by contrasting in the HXcc, the average LTC condensing heat transfer rate ($\dot{Q}_{kL}$), calculated using equation 30, versus the average HTC evaporating heat transfer rate ($\dot{Q}_{oH}$), calculated using equation 31. Of the 14.400 cycles calculated, 49.6 % are in the range of ± 5 % of accordance and 89.4 % are in

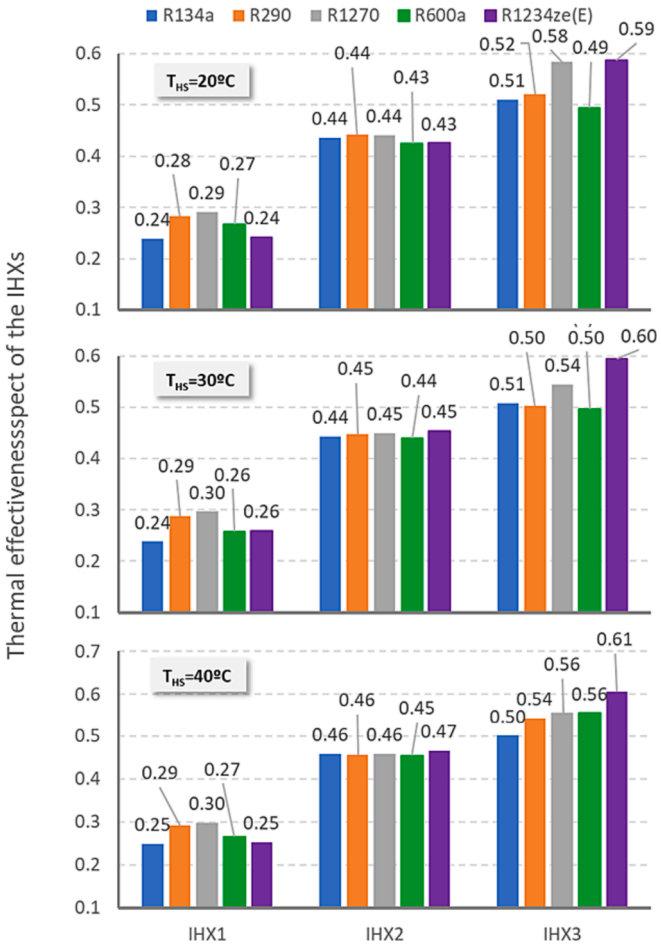

Fig. 6. Thermal effectiveness of the IHXs.

Table 6
Phase Change Temperatures, Compression ratios and compressor discharge temperatures.

Refrigerant pair	Heat sink temp.	IHX	T_{kH} (°C)	T_{oH} (°C)	T_{kL} (°C)	T_{oL} (°C)	r_{cH} (°C)	r_{cL} (°C)	$\Delta T_{IHX,\ liq}$ (°C)	$\Delta T_{IHX,vap}$ (°C)	T_{disH} (°C)	T_{disL} (°C)
R134a/R744	20	BASE	26.88	−14.37	−9.01	−28.67	4.31	1.87	0.00	0.00	69.88	80.24
		IHX1	26.44	−14.71	−9.37	−29.06	4.42	1.88	−4.89	4.92	75.81	81.43
		IHX2	26.25	−15.98	−10.59	−28.95	4.51	1.81	−7.50	17.6	71.13	86.92
		IHX3	26.85	−14.68	−9.17	−29.04	4.36	1.89	−0.15	4.27	70.11	82.35
	30	BASE	36.82	−12.07	−5.78	−28.33	5.18	2.02	0.00	0.00	81.64	94.49
		IHX1	36.37	−12.28	−6.09	−28.52	5.29	2.02	−5.95	6.21	88.66	93.87
		IHX2	36.12	−13.78	−6.95	−28.35	5.44	1.96	−8.19	21.3	83.47	101.14
		IHX3	36.53	−12.61	−5.97	−28.63	5.25	2.03	−0.07	4.73	83.00	98.47
	40	BASE	46.79	−9.24	−2.00	−27.90	6.07	2.20	0.00	0.00	92.84	106.72
		IHX1	46.42	−9.60	−2.18	−27.82	6.24	2.19	−7.11	7.86	102.70	107.50
		IHX2	46.21	−11.17	−2.65	−27.81	6.45	2.16	−8.95	26.2	95.62	116.53
		IHX3	46.80	−9.45	−2.04	−28.02	6.13	2.21	−0.11	6.26	93.39	109.91
R290/R744	20	BASE	26.38	−15.65	−9.87	−30.69	3.51	1.96	0.00	0.00	70.90	85.22
		IHX1	26.21	−16.29	−10.41	−30.84	3.57	1.94	−5.78	6.27	75.95	86.01
		IHX2	26.14	−16.75	−10.55	−30.56	3.62	1.92	−7.22	17.6	71.03	90.90
		IHX3	26.30	−15.93	−10.12	−30.53	3.52	1.94	−0.34	4.41	70.43	86.90
	30	BASE	36.29	−13.16	−5.85	−29.97	4.38	2.13	0.00	0.00	81.83	100.16
		IHX1	36.25	−12.91	−6.07	−29.96	4.29	2.12	−6.76	7.70	88.37	97.57
		IHX2	35.97	−14.52	−6.61	−29.88	4.35	2.08	−7.83	21.3	83.42	108.00
		IHX3	36.38	−12.96	−5.92	−29.85	4.37	2.12	−0.57	5.11	81.81	100.68
	40	BASE	46.79	−8.26	−1.23	−28.57	5.06	2.30	0.00	0.00	92.59	110.68
		IHX1	46.38	−9.70	−2.20	−29.01	5.01	2.27	−7.79	9.29	101.51	109.94
		IHX2	46.09	−11.02	−2.41	−28.83	5.09	2.25	−8.41	25.5	94.13	119.20
		IHX3	46.54	−9.11	−1.84	−29.31	5.13	2.32	−0.72	7.55	92.79	115.14
R1270/R744	20	BASE	26.54	−18.09	−12.10	−29.22	3.71	1.81	0.00	0.00	77.33	77.02
		IHX1	26.29	−18.07	−12.16	−30.08	3.70	1.80	−6.25	7.18	83.47	76.56
		IHX2	26.15	−19.07	−12.74	−29.89	3.80	1.76	−7.53	18.1	78.68	84.27
		IHX3	26.48	−17.98	−12.05	−29.91	3.68	1.79	0.89	2.43	77.77	79.15
	30	BASE	36.59	−14.93	−7.95	−28.95	4.25	1.95	0.00	0.00	89.99	90.74
		IHX1	36.39	−15.38	−8.55	−29.02	4.30	1.92	−6.52	7.93	97.72	89.16
		IHX2	35.96	−16.68	−9.02	−28.87	4.43	1.89	−8.17	20.4	91.68	97.26
		IHX3	36.60	−15.23	−8.04	−29.05	4.28	1.95	0.17	5.13	90.54	93.27
	40	BASE	47.08	−12.09	−3.69	−28.53	4.86	2.15	0.00	0.00	104.73	104.62
		IHX1	46.40	−12.91	−4.34	−28.59	4.94	2.12	−7.30	9.25	113.16	104.02
		IHX2	46.30	−14.03	−4.61	−28.74	5.10	2.10	−8.76	24.5	106.07	114.10
		IHX3	46.89	−12.41	−4.07	−28.75	4.89	2.14	0.03	6.50	105.17	107.60
R600a/R744	20	BASE	27.91	−12.91	−7.69	−28.43	4.32	1.93	0.00	0.00	66.14	84.04
		IHX1	27.72	−12.63	−7.70	−28.38	4.46	1.92	−5.01	5.06	70.77	84.36
		IHX2	27.46	−14.19	−9.29	−28.16	4.53	1.83	−7.57	16.2	66.60	88.83
		IHX3	27.86	−12.89	−7.79	−28.58	4.34	1.93	−0.36	4.47	65.56	84.85
	30	BASE	38.08	−10.28	−4.68	−27.99	5.12	2.06	0.00	0.00	75.34	94.58
		IHX1	38.00	−10.37	−4.82	−28.02	5.29	2.06	−5.69	5.66	80.48	94.40
		IHX2	37.92	−11.52	−5.86	−28.04	5.37	2.00	−7.63	18.7	76.43	102.25
		IHX3	38.05	−10.54	−4.80	−28.11	5.16	2.06	−0.34	5.25	75.30	96.65
	40	BASE	47.11	−7.37	−0.61	−27.55	5.97	2.26	0.00	0.00	85.52	108.94
		IHX1	46.70	−8.20	−1.25	−27.51	6.08	2.21	−7.59	7.97	92.84	109.37
		IHX2	47.37	−9.66	−2.04	−27.68	6.37	2.19	−9.38	25.3	87.18	119.70
		IHX3	47.08	−8.24	−1.11	−27.71	5.99	2.24	−0.33	7.04	86.00	111.48
R1234ze(E)/R744	20	BASE	28.05	−13.64	−8.29	−28.67	4.57	1.91	0.00	0.00	63.83	81.63
		IHX1	28.47	−13.42	−8.27	−28.60	4.78	1.91	−5.53	5.40	71.27	82.46
		IHX2	28.31	−14.88	−9.75	−28.68	4.83	1.84	−6.79	17.5	65.24	87.12
		IHX3	27.57	−14.48	−9.18	−28.91	4.66	1.88	−0.29	4.24	65.86	83.22
	30	BASE	38.17	−10.84	−5.20	−27.93	5.42	2.03	0.00	0.00	76.05	93.99
		IHX1	37.69	−10.90	−5.49	−28.11	5.59	2.03	−6.73	7.08	83.11	93.81
		IHX2	37.46	−12.44	−6.43	−28.15	5.66	1.97	−7.69	22.1	79.84	101.88
		IHX3	37.97	−10.79	−5.03	−28.01	5.39	2.04	−0.56	5.82	78.42	97.70
	40	BASE	48.07	−8.38	−1.41	−27.37	6.39	2.19	0.00	0.00	87.17	108.29
		IHX1	47.59	−8.45	−1.94	−27.50	6.51	2.17	−7.78	8.2	95.75	110.44
		IHX2	47.59	−9.70	−2.15	−27.29	6.67	2.15	−8.16	26.5	89.39	117.67
		IHX3	48.01	−8.57	−1.73	−27.56	6.44	2.19	−0.73	7.05	87.47	111.74

the range of ± 10 % of accordance. In view of these results together with the standard deviations shown in Table 4, the high confidence value in the experimental data acquired is evidenced.

5. Analysis related to cycle parameters

As mentioned in previous sections, this work is focused on analyzing the energy influence that the IHX has on the CRS. To attain this objective three locations of the IHX have been studied in comparison with the BASE configuration, in which none IHX is connected. In the named IHX1 configuration, the IHX is located in the HTC and brings into thermal contact its liquid and suction lines. In configuration named IHX2, the IHX brings into thermal contact the HTC liquid line with the LTC suction line. Finally, in the called IHX3 configuration, the IHX is placed in the LTC and thermally connects its liquid and suction lines. Each configuration has been analyzed at three different heat sink temperatures (20 °C, 30 °C and 40 °C) and at the same heat source temperature (-20 °C) with the five before mentioned refrigerant pairs, which has resulted in sixty tests that have generated a great quantity of information.

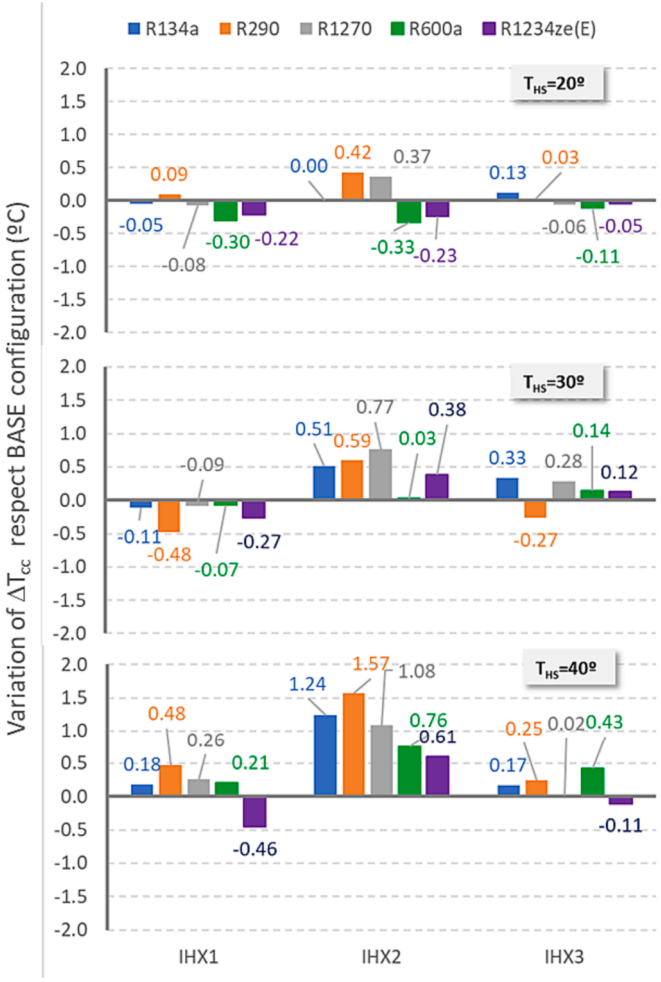

Fig. 7. Variations of Temperature difference in the cascade heat exchanger.

By introducing the IHX, the direct effects on the cycle parameters are the temperature reduction at the expansion valve inlet and the temperature increase at the compressor suction port. These direct effects trigger a series of side effects on other parameters, such as the reduction of the vapour quality at evaporator inlet, the increase of the specific cooling production, and the increase of both the compressor suction specific volume and its discharge temperature. Finally, the refrigerant mass flow rate and phase change temperatures are also affected.

Fig. 6 shows the thermal effectiveness (ε_{IHX}) of each IHX tested at the three heat sink temperatures. We can observe that the values obtained for IHX, are not function of the heat sink temperature. The IHX3 presents the greatest values, while the IHX1 the lowest, considering that both has the same heat transfer surface, this is a proof of the better heat transfer properties of R744 respect the other refrigerants.

If we look at the ε_{IHX1} values, the three hydrocarbons, especially R1270, generate higher levels than those obtained with the R134a and R1234ze(E), while the ε_{IHX2} values are very similar among all the refrigerants. As for the values of ε_{IHX3} values, it seems from the represented data that R744 works with better heat transfer conditions when R1234ze (E) and R1270 are charged in the HTC.

In case of the CRS, when an IHX is activated, it has a direct influence on the cycle in which it is mounted, but also an indirect influence on the other cycle, this is the case for IHX1 and IHX3, however the IHX2 has a direct influence on both cycles. In this section we show these direct and indirect effects.

The subcooling and superheating produced in liquid and vapour lines are calculated with equations 37 and 38, respectively, and their values are shown in Table 6. It is observed that the IHX2 generates the greatest subcooling and superheating values in the HTC and LTC, respectively. In addition, these values are higher as the heat rejection temperature increases.

Regarding the phase change temperatures, they were calculated using equations 18 to 21 and their values are collected also in Table 6. The phase change temperatures in the HT condenser (T_{kH}) and in the low temperature evaporator (T_{OL}) do not undergo considerable changes, always reductions below 1 °C, whichever the IHX activated, and the heat sink temperature tested. The evaporating temperature in the HTC (T_{OH}) and the condensing temperature in the LTC (T_{kL}), show the same trend as T_{kH} and T_{OL} with the activation of the IHX1 and the IHX3, but experience higher reductions when the IHX2 is activated, specially the T_{OH}.

According to these small variations in phase change temperatures, other parameters such as compression ratios, and cascade heat exchanger temperature difference (ΔT_{cc}) vary. In the case of compression ratios, they suffer minor variations with the activation of the IHXs, as can be deduced from data in Table 6. In general, the highest increments occur with IHX2, and the lowest with IHX3. In particular, the r_{cH} frequently undergoes increases (by around 4 %, 1.8 % and 0.7 % in average with IHX2, IHX1 and IHX3 respectively), while r_{cL} undergoes decreases, but in lower value (by around −2.9 %, −0.68 % and −0.13 % in average with IHX2, IHX1 and IHX3 respectively). No particular trends are found between the variations of the compression ratios and the heat sink temperature variation. With regard to the cascade heat exchanger temperature difference, there are no significant variations when IHX1 and IHX3 are activated (minor than 0.5 °C), only the IHX2 generates increases greater than 1 °C at 40 °C of heat sink temperature, as is observed in Fig. 7. It is observed that variations in ΔT_{cc} are higher as higher the heat sink temperature is.

The compressor discharge temperatures shown in Table 6, vary more significantly than the phase change temperatures. Thus, when IHX1 is activated, the TdisH increases by an average of 8 %±1.3 %, while TdisL hardly varies. When IHX2 is activated, TdisH increases by 2 %±1% on average, while TdisL rises by 8 %±0.9 % on average. The IHX3 produces 0.7 %±1% average variations in TdisH and 2.6 %±0.9 % average variations in TdisL. The increment in TdisL and TdisH makes these temperatures exceed in several cases 100 °C. This will not be a problem if the facility operates in a cycling mode, since the compressor does not reach such high temperatures because it is not running all the time, as pointed out by [4].

Another observation from this data is that each IHX produces a variation in both, the discharge temperature of the compressor directly affected by the superheating in the suction line, and the discharge temperature of the compressor placed in the other cycle, the latter in minor quantity. This matter is not considered in the theoretical model.

With respect to other cycle parameters, like specific cooling capacities, volumetric cooling capacities, specific compression works and refrigerant mass flow rates, all the values obtained from the experimental data are gathered in the left-hand columns of Table 7. If we focus firstly on IHX1 compared to the BASE configuration, we find that the subcooling produced by the IHX1 leads to a higher q_{oH} increment the higher the T_{SH}, thus, the increase ranges from an average of 4.38 % at 20 °C of TSH to an average of 8.66 % at 40 °C of T_{SH}. This effect also makes the q_{oL} going up but in much lower average values, by 0.23 % and 0.92 % at T_{SH} 20 °C and 40 °C respectively. Despite this increment in q_o, the superheating in the suction line is higher and, in consequence, the increase in the specific suction volume is very high, so the volumetric cooling capacities decrease by −2.16 % at T_{SH}:20 °C to 0.2 % at T_{SH}:40 °C. Regarding with the mass flow rate, the IHX1 reduces $\dot{m}_{ref,H}$ an average that ranges from −4.63 % to −6.85 % at 20 °C and 40 °C of T_{HS} respectively, but also affects the $\dot{m}_{ref,L}$ generating a slight increase (around a 0.2 % on average at 20 °C of T_{SH} to 0.9 % on average at 40 °C of T_{SH}). For its part, the specific compression work decreases by −3.11 %

Table 7
Main thermodynamic cycle and energy parameters of the CRS.

Refrigerant pair	Heat sink temp.	IHX	$\dot{m}_{ref,H}$(kg·h^{-1})	$\dot{m}_{ref,L}$(kg·h^{-1})	$q_{O,H}$ (kJ·kg^{-1})	$q_{O,L}$ (kJ·kg^{-1})	$q_{v,H}$ (kJ·m^{-3})	$q_{v,L}$ (kJ·m^{-3})	$w_{c,H}$ (kJ·kg^{-1})	$w_{C,L}$ (kJ·kg^{-1})	$\eta_{G,H}$ (-)	$\eta_{G,L}$ (-)	$\dot{Q}_{O,H}$(kW)	$\dot{Q}_{O,L}$(kW)	COP_H (-)	COP_L (-)	COP (-)
R134a/R744	20	BASE	37.89	19.57	165.7	265.6	1310	9,241	54.70	85.34	0.484	0.250	1.744	1.444	2.476	2.284	1.081
		IHX1	35.74	19.88	172.7	266.2	1264	9,144	53.37	86.83	0.495	0.246	1.714	1.470	2.490	2.322	1.113
		IHX2	34.87	19.34	176.3	269.2	1310	8,381	56.82	74.88	0.475	0.264	1.708	1.446	2.505	2.391	1.124
		IHX3	37.32	19.75	165.4	268.3	1292	8,988	55.09	83.35	0.481	0.256	1.714	1.472	2.438	2.328	1.102
	30	BASE	39.51	19.54	152.9	257.6	1310	8,976	60.78	96.13	0.516	0.261	1.678	1.398	2.137	2.122	0.968
		IHX1	37.52	19.84	162.2	258.4	1281	8,942	58.61	95.61	0.533	0.261	1.690	1.424	2.195	2.163	0.997
		IHX2	36.28	18.95	165.3	261.0	1319	8,071	62.94	81.76	0.511	0.283	1.666	1.374	2.210	2.163	0.989
		IHX3	38.38	19.08	153.2	261.4	1279	8,765	61.42	95.37	0.511	0.257	1.633	1.385	2.091	2.064	0.954
	40	BASE	41.66	19.25	138.1	248.2	1300	8,746	66.34	10,579	0.538	0.268	1.599	1.327	1.819	1.933	0.848
		IHX1	38.79	19.26	151.6	248.8	1293	8,798	64.73	106.5	0.559	0.272	1.633	1.331	1.913	1.961	0.869
		IHX2	37.55	18.81	153.8	249.9	1334	7,666	68.88	89.41	0.533	0.306	1.604	1.305	1.922	1.966	0.871
		IHX3	41.03	19.27	138.5	251.7	1289	8,546	66.90	103.1	0.536	0.277	1.578	1.347	1.806	1.971	0.865
R290/R744	20	BASE	18.59	21.35	314.4	268.2	1846	8,574	109.5	88.75	0.429	0.298	1.624	1.591	2.131	2.584	1.155
		IHX1	17.76	21.51	329.1	271.2	1824	8,463	106.9	86.42	0.442	0.305	1.624	1.621	2.179	2.670	1.199
		IHX2	17.83	21.09	332.5	269.8	1896	7,892	113.1	77.88	0.422	0.313	1.647	1.580	2.174	2.591	1.156
		IHX3	18.55	21.34	313.7	270.2	1841	8,512	110.6	87.21	0.427	0.298	1.616	1.602	2.118	2.608	1.163
	30	BASE	19.06	20.25	290.1	258.6	1713	8,421	120.7	99.89	0.481	0.305	1.536	1.455	1.839	2.222	0.976
		IHX1	18.67	21.01	309.5	259.2	1773	8,473	115.0	97.90	0.495	0.314	1.605	1.513	1.951	2.323	1.026
		IHX2	17.81	20.05	311.4	260.0	1842	7,613	125.4	87.78	0.457	0.328	1.541	1.448	1.892	2.239	0.991
		IHX3	19.21	20.11	289.9	261.3	1715	8,343	119.8	96.31	0.484	0.310	1.547	1.460	1.849	2.254	0.983
	40	BASE	21.37	19.71	266.7	246.7	1696	8,432	126.7	107.5	0.531	0.315	1.526	1.350	1.668	1.975	0.827
		IHX1	19.51	20.06	288.8	249.3	1743	8,361	125.2	106.9	0.526	0.322	1.499	1.390	1.705	2.062	0.873
		IHX2	19.07	19.49	289.1	249.8	1814	7,391	133.7	91.65	0.492	0.350	1.469	1.352	1.681	2.004	0.853
		IHX3	20.66	20.00	265.9	251.9	1664	8,121	128.9	106.7	0.523	0.337	1.469	1.400	1.629	2.062	0.867
R1270/R744	20	BASE	20.15	21.34	316.6	273.8	2084	8,961	115.6	82.28	0.450	0.265	1.772	1.623	2.068	2.713	1.115
		IHX1	19.66	21.51	329.5	273.5	2058	8,983	110.5	82.05	0.470	0.266	1.799	1.634	2.137	2.746	1.137
		IHX2	19.22	20.87	331.3	274.8	2106	8,241	118.8	72.62	0.444	0.276	1.769	1.593	2.093	2.701	1.110
		IHX3	20.14	21.20	313.6	273.0	2071	8,815	116.3	80.58	0.448	0.268	1.754	1.608	2.047	2.712	1.109
	30	BASE	21.07	20.59	298.7	263.0	2155	8,964	127.0	93.42	0.473	0.254	1.748	1.504	1.831	2.339	0.941
		IHX1	19.87	20.82	316.7	264.4	2127	8,966	124.0	91.69	0.486	0.254	1.748	1.530	1.874	2.434	0.980
		IHX2	19.41	20.27	318.9	265.5	2168	8,058	131.3	78.84	0.466	0.278	1.720	1.495	1.863	2.457	0.976
		IHX3	20.72	20.42	298.5	265.0	2132	8,801	128.3	92.20	0.468	0.252	1.718	1.503	1.800	2.305	0.936
	40	BASE	21.52	20.26	276.1	252.9	2160	8,675	141.9	103.3	0.481	0.272	1.650	1.423	1.552	2.165	0.827
		IHX1	20.14	20.15	297.2	254.4	2121	8,708	138.1	103.0	0.498	0.267	1.663	1.424	1.603	2.174	0.841
		IHX2	19.83	20.03	299.1	254.9	2191	7,654	145.9	89.00	0.476	0.303	1.648	1.418	1.606	2.197	0.848
		IHX3	21.25	20.23	276.1	255.8	2137	8,483	143.0	102.0	0.480	0.272	1.629	1.437	1.540	2.160	0.834
R600a/R744	20	BASE	20.35	19.28	300.8	262.5	747	9,233	105.3	88.89	0.416	0.251	1.701	1.406	2.166	2.143	0.976
		IHX1	19.57	19.32	314.5	262.5	732	9,261	100.8	89.28	0.428	0.249	1.710	1.409	2.202	2.127	0.979
		IHX2	19.18	18.59	321.2	266.3	757	8,582	106.7	77.64	0.417	0.263	1.711	1.375	2.240	2.193	0.989
		IHX3	20.36	19.44	302.6	266.2	751	9,079	103.9	85.40	0.424	0.267	1.711	1.438	2.212	2.249	1.018
	30	BASE	20.82	19.52	288.8	255.6	783	9,072	113.1	96.74	0.456	0.268	1.670	1.386	2.013	2.089	0.928
		IHX1	19.81	19.47	303.2	255.7	763	9,068	108.5	96.79	0.473	0.269	1.668	1.383	2.066	2.111	0.946
		IHX2	19.25	18.69	309.4	258.7	785	8,225	111.8	85.64	0.452	0.287	1.654	1.343	2.048	2.074	0.923
		IHX3	20.53	19.50	288.3	258.9	774	8,881	113.3	93.79	0.458	0.274	1.644	1.403	2.008	2.146	0.953
	40	BASE	21.67	18.35	260.7	244.9	743	8,766	122.4	107.4	0.488	0.275	1.569	1.249	1.746	1.809	0.786
		IHX1	20.46	18.42	281.5	246.5	747	8,837	119.5	108.2	0.486	0.261	1.600	1.261	1.777	1.778	0.784
		IHX2	20.19	18.30	283.1	248.5	766	7,689	129.1	93.28	0.470	0.295	1.588	1.263	1.770	1.816	0.793
		IHX3	21.54	18.42	261.2	250.6	745	8,592	125.1	104.1	0.484	0.279	1.563	1.282	1.740	1.867	0.809
R1234ze(E)/R744	20	BASE	42.18	20.26	150.5	264.0	980	9,200	52.65	86.48	0.439	0.262	1.763	1.486	2.201	2.321	1.031
		IHX1	40.02	19.79	157.1	263.8	952	9,207	52.14	87.32	0.440	0.256	1.747	1.450	2.149	2.248	0.995
		IHX2	39.22	19.53	158.8	267.2	985	8,404	54.69	74.63	0.429	0.274	1.730	1.449	2.194	2.382	1.038
		IHX3	40.45	19.29	150.4	268.5	949	9,044	55.41	84.38	0.416	0.255	1.690	1.439	2.063	2.307	0.997
	30	BASE	44.50	19.55	137.3	256.0	987	9,076	59.44	96.35	0.460	0.263	1.698	1.390	1.876	2.113	0.890
		IHX1	41.44	19.63	148.7	256.9	972	9,048	56.71	96.27	0.468	0.263	1.712	1.401	1.922	2.123	0.903
		IHX2	40.73	19.11	148.5	259.2	1002	8,094	64.21	82.38	0.429	0.288	1.681	1.376	1.841	2.169	0.889
		IHX3	44.55	20.35	138.0	259.0	991	8,928	61.72	94.89	0.434	0.268	1.708	1.464	1.784	2.176	0.898
	40	BASE	46.00	19.24	124.7	246.7	975	8,888	65.58	107.2	0.472	0.269	1.593	1.318	1.583	1.936	0.782
		IHX1	42.92	19.80	136.7	251.6	977	8,728	62.86	103.9	0.479	0.271	1.630	1.384	1.637	1.985	0.818
		IHX2	42.62	19.16	136.4	248.4	1006	7,771	68.55	90.51	0.463	0.302	1.615	1.322	1.654	1.965	0.802
		IHX3	45.55	19.14	124.4	251.5	964	8,697	66.00	104.9	0.470	0.272	1.573	1.337	1.565	1.957	0.792

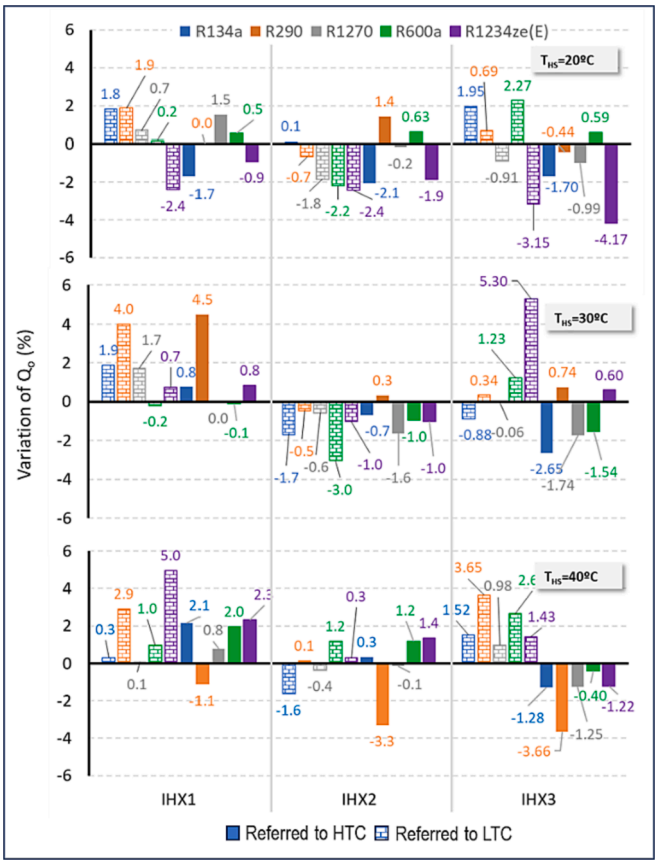

Fig. 8. Variation of Evaporator cooling capacity introduced by the IHXs respect to the BASE configuration.

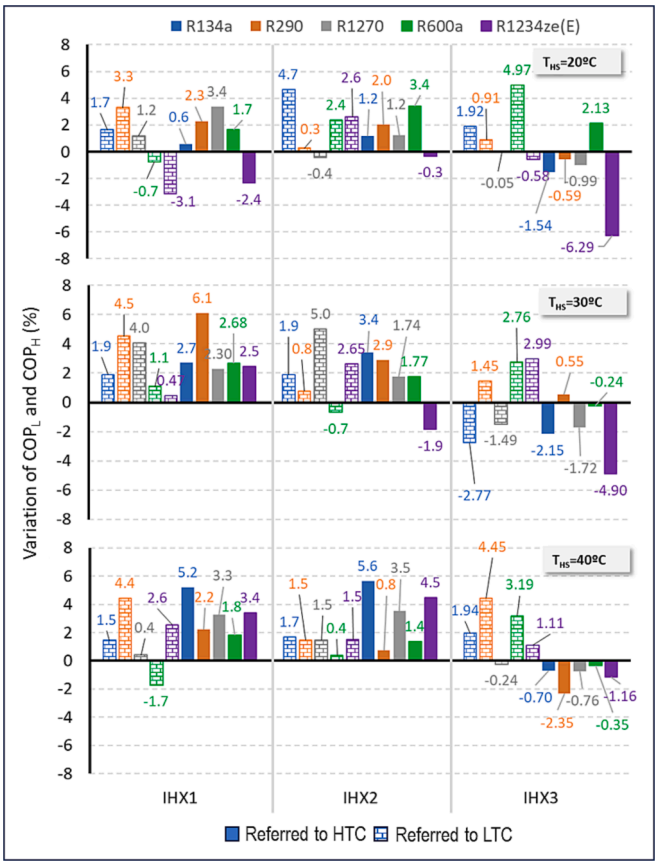

Fig. 9. Variation of the COP_L and COP_H introduced by the IHXs respect to the BASE configuration.

on average in the HTC, and by −0.44 % on average in the LTC. In the case of w_{cH}, this reduction is due to the effect in semi-hermetic reciprocating compressors explained by Sánchez et al. [18]. It consists in the fact that the higher the refrigerant temperature and/or the refrigerant mass flow rate at the compressor inlet, the lower the heat that the refrigerant absorbs from the electric motor, and, therefore, the lower the superheat at the compressor suction port, what leads to reduce the actual specific compression work. This effect is more evident in the case of IHX2.

The values obtained with IHX2 compared to BASE configuration show that the IHX makes an important subcooling in the liquid line of the HTC, this is the reason why the q_{oH} rises even more than with the IHX1, by an average of 5.82 % at 20 °C of T_{SH} to an average of 9.2 % at 40 °C of T_{SH}. Likewise, the q_{oL} increases when IHX2 is activated, but by a milder amount than q_{oH}, by 1.0 % in average for the three TSH tested. The superheating produced by the IHX2 in the LTC suction line is so high that the q_{vL} goes down by −8.2 % at T_{SH}:20 °C and by −12.26 % at T_{SH}:40 °C on average. A way higher reduction than that produced by IHX1 in the q_{vH}. When IHX2 is connected the q_{vH} increases due to the high increase in q_{oH}. This increment fluctuates between 1.1 % and 3.5 % at 20 °C and 40 °C respectively. The refrigerant mass flow rate is reduced in a range between −5.9 % to −8.5 % on average in the HTC and between –2.4 % to −1.0 % on average in the LTC, both cases at 20 °C and 40 °C of T_{SH} respectively. As for specific compression works, the w_{cL} decreases between −12.5 % and −14.6 % on average, while the w_{cH} increases from 3.0 % to 4.4 % when the T_{SH} varies from 20 °C to 40 °C. In both cases, the variations are due to the same facts explained by Sánchez et al. [18] and commented on the previous paragraph.

The last IHX to evaluate its effects on both cycle parameters is the IHX3. The effects of activating IHX3 are different on the LTC, than the effects of IHX1 on the HTC, thus while at T_{SH}:40 °C the IHX1 increases q_{oH} by 8.7 % in mean, the IHX3 make increase q_{oL}, by 1.8 % in mean, but the superheating is higher because the qv, also at T_{SH}:40 °C, the IHX1 produces an increase by 0.2 % in mean in q_{vH} while the IHX3 produces a decrease by −2.5 % in mean in q_{vL} due to the additional superheating at compressor suction port (by 5.3 °C on average). The HX3 reduces the w_{cL} by −1.9 % on average at TSH:40 °C, while the IHX1 causes the w_{cH} to reduce −2.6 % on average at the same T_{SH}. Respect to the w_{cH} when the IHX3 is operating, it increases by 1.2 %, due to the refrigerant mass flow reduction, by −1.54 %.

Despite using three different compressors in the HTC, the compressor global efficiency values, calculated using equation 33, are very similar. Thus, with the compressor BITZER 2HES-1Y-40S, used with R134a, the mean value obtained is 51.43 %±1.04 %, with the compressor DORIN H-80CC, used with R290 and R1270, the average value obtained is 47.29 % ±1.2 %, and with the compressor BITZER 2EC-2-2Y-40S, used with R600a and R1234ze(E), the mean value obtained is 45.21 %±1.01 %. As for the compressor DORIN CD150H, used in the LTC, the average value calculated with equation 32 is 27.84 %±1.14 %. Other relevant aspects related to the compressor global efficiency are that the IHX2 increases the η_{GL} respect to the BASE value (this increase is higher as the TSH increases) and reduces the η_{GH}, while the IHX1 increases the η_{GH} having a low impact on the η_{GL}. The influence of the IHX3 on the global efficiency of the LTC and HTC is negligible.

Finally, values of the main energy parameters of the CRS calculated with the experimental data are shown in the right-hand columns of Table 7. Fig. 8 shows the cooling capacity variations of both cycles when the IHXs are activated, with respect the BASE cycle.

When the variations of the refrigerant mass flow rates and specific cooling capacities produced by the IHXs are combined, they result into the final cooling capacity of each cycle. It is observed that all the refrigerants have not the same results. Thus, when IHX1 is activated $\dot{Q}_{o,L}$

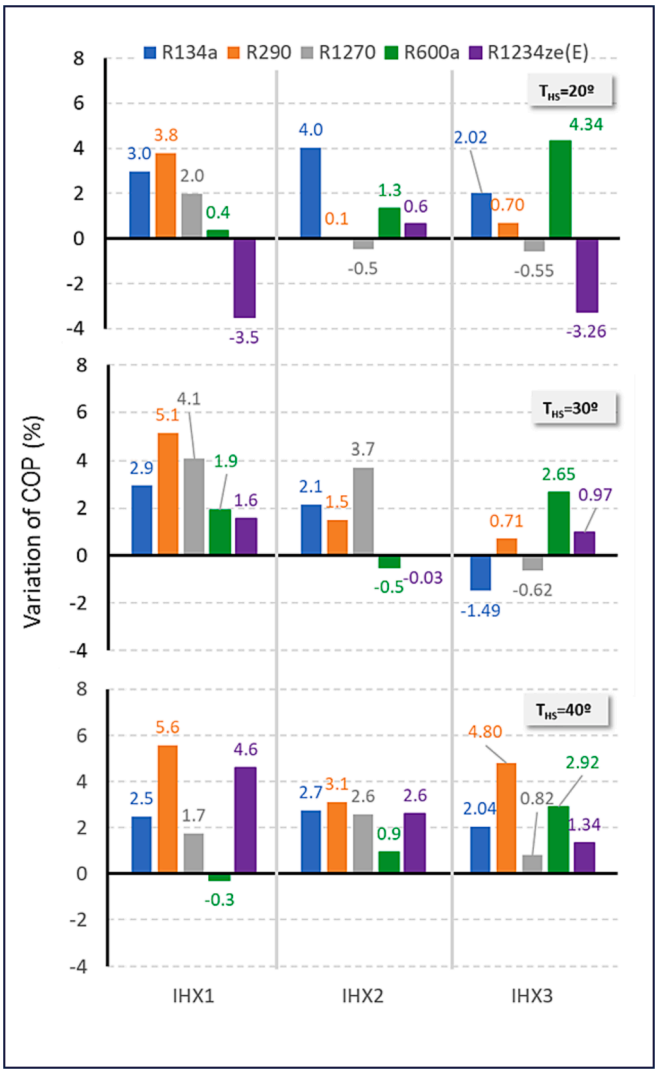

Fig. 10. Variations in the COP of the CRS introduced by the IHXs respect to the BASE configuration.

increases with the refrigerant pairs R134a/R744, R290/R744 and R1270/R744 over the entire T_{SH} range tested, but the pair R1234ze(E)/R744 presents a great increment at T_{SH}:40 °C and a decrement at T_{SH}:20 °C, while the pair R600a/R744 does not show important variations. However, the activation of the IHX2 drives to a general reduction in $\dot{Q}_{O,L}$, in all the refrigerant pairs, except at TSH:40C where very slight increases are shown. The effect of the IHX3 increases $\dot{Q}_{O,L}$, over the entire T_{SH} range, for the refrigerant pairs R134a/R744, R290/R744 and R600a/R744, while for refrigerant pairs R1234ze(E)/R744 and R1270/R744, it seems to increase at medium and high TSH values.

In conclusion, in terms of $\dot{Q}_{O,L}$, among the five refrigerant pairs, R290/R744 is the one that takes better advantage with the IHXs connection, it gets the highest improvement in $\dot{Q}_{O,L}$ when the IHX1 is connected, by 2.93 % on average, the lowest decrement when IHX2 is connected in average (by −0.37 %), and the second with higher increments (by 1.56 % in average), after the pair R600a/R744 (by 2.05 % in average).

Fig. 9 shows the variations of the LTC and HTC energy efficiencies, that is, COP_L and COP_H, respectively. In general, the effects of the IHX1 and the IHX2 are positive both for COP_L and for COP_H, only the pairs R1234ze(E)/R744 and R600a/R744 present slight decrements in some tests. The biggest increment achieved with IHX1 occurs when refrigerant pair R290/R744 is used at TSH30°C, and the biggest increment achieved

Table 8
Average variations on COP and $\Delta\dot{Q}_{O,L}$ respect the BASE configuration.

	IHX1		IHX2		IHX3	
	ΔCOP	$\Delta\dot{Q}_{O,L}$	ΔCOP	$\Delta\dot{Q}_{O,L}$	ΔCOP	$\Delta\dot{Q}_{O,L}$
R134a/R744	2.80	1.33	2.93	−1.07	0.86	0.86
R290/R744	4.83	2.93	1.57	−0.37	2.07	1.56
R1270/R744	2.60	0.83	1.93	−0.93	−0.12	0.00
R600a/R744	0.67	0.33	0.57	−1.33	3.30	2.05
R1234ze(E)/R744	0.90	1.10	1.06	−1.03	−0.32	1.19

with IHX2 when refrigerant pair R134a/R744 is used at TSH:40 °C. No special trend is found with T_{SH}. In terms of the effects caused by IHX3, it can be said that the COP_H is reduced in almost all the tests, while the COP_L is increased when R600a/R744, R290/R744 and R1234ze(E)/R744 are used, but is slightly reduced in all tests with R1270/R744 refrigerant pair and present a fluctuating trend with R134a/R744.

To conclude the analysis, Fig. 10 depicts the variations in the COP of the CRS. An overall positive effect on the COP is obtained with the three IHXs, with the highest improvements being the ones measured with the refrigerant pairs R290/R744 and R1234ze(E)/R744 at TSH:40 °C when IHX1 is activated. Only the pair R1234ze(E)/R744 at Tsh:20 °C presents a clear negative effect both with IHX1 and IHX3. Looking separately at each IHX, the pair R290/R744 presents the best behaviour with IHX1, followed by R134a/R744 and R1270/R744, being the average improvements by 4.8 %, 2.8 % and 2.6 %, respectively. The R600a/R744 and R290/R744 show the greatest mean improvements in COP, by 3.3 % and 2.07 % in average, with the IHX3. While R134a/R744 and R290/R744 show the best COP increases, by 2.9 % and 1.57 % in average, when IHX2 is activated. Therefore, the highest improvements are achieved with the IHX1, and the R290/R744 is the refrigerant pair that takes a greatest advantage from the IHX use.

6. Conclusions

For the first time, the only three possible locations of an IHX in a cascade refrigeration system have been tested. Their effects on the energy performance of each single vapor compression cycle and on the overall cascade refrigeration system have been analysed, theoretically and experimentally, using a CRS working with the refrigerants pairs R290/R744, R1230/R744, R600a/R744, R134a/R744 and R1234ze(E)/R744 in a wide range of THS (from 40 °C to 20 °C) and −20 °C as heat source temperature.

While the theoretical model predicts a worsening in the energy performance of the CRS in all the scenarios modelled, the experimental results show the opposite behaviour. This radical discrepancy is based on the heat transfer phenomena, and on the propagation of the effects of the IHXs from one cycle to another, because the theoretical model does not take them into account, and the experimental results do.

From experimental measurements it is observed that in general, the phase change temperatures and, in consequence, the temperature difference in the cascade heat exchanger and the compression ratios do not undergo significant variations, regardless the IHX connected and the T_{SH}. The discharge temperatures of the compressors whose suction lines are superheated by the IHX increase, but to a lesser extent than expected, because of the collateral effects introduced by the cooling of the electric motor winding. The same side effect influences the variations of the specific compression work. Therefore, the IHX1 reduce it in both cycles, especially in the HTC, the IHX3 reduce the w_c of the LTC, but makes the w_c of the HTC to increase, and the IHX2 produce the same effects than IHX3 related to w_c but to a greater extent. As for the specific cooling capacity and the volumetric cooling capacity, the IHX1 and IHX3 increase the former and decrease the latter, in both cycles, but to a higher amount in the cycle where they are located. The IHX2 increase the q_o in both cycles, but the q_v decreases in a large amount in the LTC and increase in the HTC. Finally, the cooling capacity of the LTC, that is, the

cooling capacity of the CRS, is increased by the IHX1 and IHX3 and is decreased by the IHX2, while the COP is increase by the three IHXs.

However, the impact of the IHXs is not equal for all the refrigerant pairs. In this sense, Table 8 gathers the mean variations on COP and $\dot{Q}_{O,L}$ with respect to the BASE configuration. It is observed that the pair R290/R744 presents the best improvement in COP and in $\dot{Q}_{O,L}$ when IHX1 is activated, while when IHX2 is operating, is the pair R134/R744 the one that presents the highest improvement in COP and the pair R290/R744 the one with the lowest $\dot{Q}_{O,L}$ reduction. The pair R600a/R744 takes best advantage of the IHX3 activation, followed by the pair R290/R744.

CRediT authorship contribution statement

Ramón Cabello: Conceptualization, Formal analysis, Funding acquisition, Methodology, Supervision, Writing – original draft, Writing – review & editing. **Alejandro Andreu-Nácher:** Formal analysis, Investigation, Validation, Visualization, Writing – original draft. **Daniel Sánchez:** Conceptualization, Methodology, Resources, Supervision, Validation, Writing – original draft. **Rafael Larrondo:** Formal analysis, Methodology, Validation.

Declaration of competing interest

The authors declare that they have no known competing financial interests or personal relationships that could have appeared to influence the work reported in this paper.

Data availability

Data will be made available on request.

Acknowledgements

The authors gratefully acknowledge the “Ministerio de Ciencia y Tecnología” of Spain (project RTI2018-093501-B-C21) and the Spanish Ministry of Science and Innovation (PID2021-126926OB-C21) for financing this research work. The authors would like also to acknowledge the economic support to this study by the European Union – “NextGenerationEU” through the grant INVEST/2022/294 to R. Larrondo.

References

[1] P.K. Bansal, S. Jain, Cascade systems: Past, present, and future, ASHRAE Trans. 113 (2007) 245–252. ISSN: 00012505.
[2] F.W.A. Blanco, M.V. Almeida, D.F. Marcucci, J.A. dos Reis, E.P. Bandarra, Experimental evaluation of low-GWP refrigerants R513A, R1234yf and R436A as alternatives for R134a in a cascade refrigeration cycle with R744, Int. J. Refrig. 144 (2022) 175–187, //doi.org/10.1016/j.ijrefrig.2022.08.010.
[3] R. Cabello, D. Sánchez, D. Llopis, A. Andreu-Nacher, D. Calleja-Anta, Energy impact of the Internal Heat Exchanger in a horizontal freezing cabinet. Experimental evaluation with the R404A low-GWP alternatives R454C, R455A, R468A, R290 and R1270, Int. J. Refrig. 137 (2022), pp 22-33. //doi.org/10.1016/j.ijrefrig.2022.02.007.
[4] R. Cabello, D. Sánchez, R. Llopis, A. Andreu-Nacher, D. Calleja-Anta, Energy impact of the Internal Heat Exchanger in a horizontal freezing cabinet. Experimental evaluation with the R404A low-GWP alternatives R454C, R455A, R468A, R290 and R1270, Int. J. Refrig 137 (2022) 22–33, https://doi.org/10.1016/j.ijrefrig.2022.02.007.
[5] R. Cabello, A. Andreu-Nácher, A. Sánchez, R. Llopis, F. Vidan-Falomir, Energy comparison based on experimental results of a cascade refrigeration system pairing R744 with R134a, R1234ze(E) and the natural refrigerants R290, R1270, R600a, Int. J. Refrig (2023), https://doi.org/10.1016/j.ijrefrig.2023.01.009.
[6] H.W. Coleman, W.G. Steele, Experimentation, validation and uncertainty analysis for engineers, 4th Edition, John Wiley & Sons, 2018. ISBN: 9781119417514.
[7] G. Dreyfus, N. Borgford-Parnell, J. Christensen, D.W. Fahey, B. Motherway, T. Peters, R. Picolotti, N. Shah, Y. Xu, Assessment of climate and development benefits of efficient and climate-friendly cooling. Molina, M., and Zaelke, D., Steering Committee Co-Chairs, 2020. Available at: https://ccacoalition.org/en/resources/assessmentclimate-and-development-benefits-efficient-and-climate-friendly-cooling.
[8] J.L. Dupont, The Role of Refrigeration in the Global Economy (2019), 38th Note on Refrigeration Technologies, Int. Instit. Refrig. (2019), https://doi.org/10.18462/iif.NItec38.06.2019.
[9] Md.W. Faruque, M.R. Uddin, S. Salehin, M.M. Ehsan, A Comprehensive Thermodynamic Assessment of Cascade Refrigeration System Utilizing Low GWP Hydrocarbon Refrigerants, Int. J. Thermofluids 15 (2022) 100177, doi.org/10.1016/j.ijft.2022.100177.
[10] Brian A. Fricke, Vishaldeep Sharma, Omar Abdelaziz, Low Global Warming Potential Refrigerants for Commercial Refrigeration Systems“. United States, 2017. https://doi.org/10.2172/1376485. https://www.osti.gov/servlets/purl/1376485.
[11] E. Heath, “Amendment to the Montreal Protocol on Substances that Deplete the Ozone Layer” (Kigali Amendment), Int. Leg. Mater. 56 (1) (2017) 193–205, https://doi.org/10.1017/ilm.2016.2.
[12] IPU, SecCool Properties, 2007. https://www.ipu.dk/products/seccool/.
[13] E.W. Lemmon, I.H. Bell, M.L. Huber, M.O. McLinden, NIST Standard Reference Database 23: reference Fluid Thermodynamic and Transport Properties-REFPROP. Version 10.0. National Institute of Standards and Technology. Gaithersburg. Standard Reference Data Program, 2018.
[14] S. Liu, J. Wang, B. Dai, X. Yang, V. Nian, H. Li, J. Yuan, Alternative positions of internal heat exchanger for CO2 booster refrigeration system: Thermodynamic analysis and annual thermal performance evaluation, Int. J. Refrig. 131 (2021) 1016–1028, doi.org/10.1016/j.ijrefrig.2021.05.003.
[15] R. Llopis, C. Sanz-Kock, R. Cabello, D. Sánchez, L. Nebot-Andrés, J. Catalán-Gil, Effects caused by the internal heat exchanger at the low temperature cycle in a cascade refrigeration plant, Appl. Ther. Eng. 103 (2016) 1077–1086. doi.org/10.1016/j.applthermaleng.2016.04.075.
[16] R.J. Moffat, Using Uncertainty Analysis in the Planning of an Experiment, J. Fluids Eng. 107 (2) (1985) 173–1117.
[17] Official Journal of the European Union, Regulation (EU) No 517/2014 of the European Parliament and the Council of 16 April 2014 on fluorinated Greenhouse Gases and Repealing Regulation (EC) No 842/2006 (Text with EEA Relevance), 2014. available at https://eur-lex.europa.eu/legal-content/en/txt/pdf/?uri=celex:32014r0517&from=en.
[18] D. Sánchez, E. Torrella, R. Cabello, R. Llopis, Influence of the superheat associated to a semihermetic compressor of a transcritical CO2 refrigeration plant, Appl. Therm. Eng. 30 (4) (2010) 302–309, https://doi.org/10.1016/j.applthermaleng.2009.09.008.
[19] S. Soni, P. Mishra, G. Maheshwari, D.S. Verma, Theoretical energy analysis of Cascade refrigeration system using low Global warming potential refrigerants, Mater. Today: Proc. 63 (2022) 164–169, //doi.org/10.1016/j.matpr.2022.02.436.
[20] UNEP – IEA. Programme and International Energy Agency, 2020. Cooling Emissions and Policy Synthesis Report. UNEP, Nairobi and IEA, Paris. ISBN No: 978-92-807-3778-3. https://www.unep.org/resources/report/cooling-emissions-and-policy-synthesis-report.